Master's thesis

NTNU
Norwegian University of Science and Technology
Faculty of Natural Sciences
Department of Biotechnology and Food Science

Marcus Hoff Hansen

Feasibility of handheld multispectral imaging for detecting quality parameters and freshness of raw Atlantic salmon (Salmo salar L.) products

Master's thesis in Food science, Technology and sustainability
Supervisor: Jørgen Lerfall
Co-supervisor: Anita Nordeng Jakobsen
May 2023

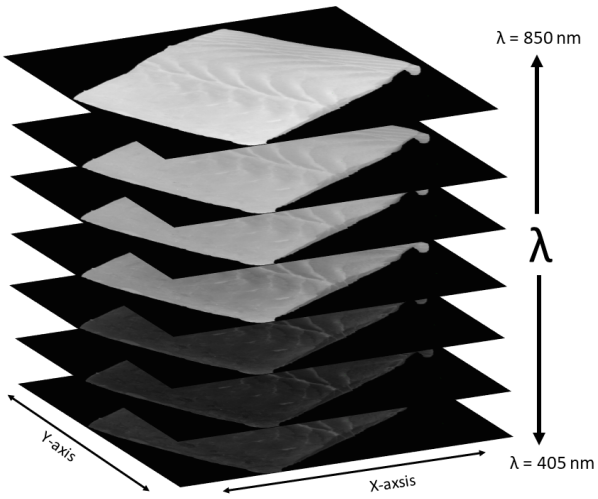

NTNU
Norwegian University of
Science and Technology

Marcus Hoff Hansen

Feasibility of handheld multispectral imaging for detecting quality parameters and freshness of raw Atlantic salmon (Salmo salar L.) products

Master's thesis in Food science, Technology and sustainability
Supervisor: Jørgen Lerfall
Co-supervisor: Anita Nordeng Jakobsen
May 2023

Norwegian University of Science and Technology
Faculty of Natural Sciences
Department of Biotechnology and Food Science

NTNU
Norwegian University of
Science and Technology

Abstract

In this thesis, a handheld multispectral imaging prototype developed by Videometer A/S for the TraceMyFish research project was used to test quality parameters of 20 salmon fillets and 30 head-on-gutted salmon samples. Multispectral data were processed and compared against established methods for colour measurements, sensory testing, and microbial growth. The ability to detect melanin spots on salmon fillets was explored and the multispectral imager prototype's ability to image directly on the samples was evaluated.

It was shown that using the handheld multispectral imaging device directly on salmon fillets gave a significant ($p<0.05$) reduction in the total spectra reflection compared to imaging of 10x10 cm fillet portions in petri dishes. Colour measurements with multispectral imaging provided lighter ($L^*=59.1\pm1.0$), more saturated ($C^*=57.3\pm1.6$) and a more yellow hue ($h^*=50.9\pm0.7$) then a RGB colour measurement device ($L^*=55.0\pm1.8$, $C^*=49.5\pm2.0$, $h^*=43.9\pm0.5$). Low differences were shown between RGB and MSI instruments when salmon fillet samples were ranked after SalmoFan™ colour card score using chroma-values (C^*), with an average difference of 0.15 in colour card score between instruments. The multispectral instrument tended to give a higher colour card score than the RGB-based device, though the max difference was at 1 score point between instruments. Measured melanin spots had significant ($p<0.05$) different reflection on all seven wavelength bands then normal salmon fillet flesh spectra, meaning that the device can easily detect melanin spots.

High correlation between multispectral data and QIM-score from head-on-gutted salmon stored on ice was achieved, with 405 nm band giving the highest negative correlation ($r=-0.792$) imaged on the abdominal skin region. Gill spectra had significant ($p<0.05$) separation of the 850 nm band between fresh (day 1), matured (day 8), and spoiled (day 17) samples and showed high positive correlation ($r=0.696$) with QIM-score. Bacterial growth also correlated highly at the 405 nm spectrum of skin in the case of APC ($r=-0.625$), *Pseudomonas ssp*. ($r=-0.744$), H_2S-producing bacteria ($r=-0.719$), and total aerobe psychrotrophic plate count ($r=-0.614$). Gill samples showed similarly high correlations ($r>0.6$) for bacterial growth at the 850 nm spectrum.

Using the multispectral imaging prototype directly on whole salmon fillets led to an increased number of variables that can impact results and is affected by bias from the operator handling the instrument. It was suggested that future designs should mitigate the impacts of these variables. The prototype was able to measure and evaluate colour of salmon flesh comparable to industrial standard colour measuring methods and detection of melanin spots was achieved. Multispectral imaging prototype showed the ability to correlate spectral data with microbial and sensory methods, and the possibility to become an excellent tool in predicting the quality and shelf life of head-on-gutted salmon.

Sammendrag

I denne oppgaven ble et håndholdt multispektral bildetaker prototype utviklet av Videometer A/S for TraceMyFish forskningsprosjektet, brukt til å teste kvalitetsparametere av 20 laksefileter og 30 hodet-på-sløyet laks. Multispektral data ble prosessert og sammenlignet med etablerte metoder for fargemåling, sensorisk testing og mikrobiell vekst. Evnen til å detektere melaninflekker på laksefileter ble også utforsket og det multispektrale billedtakning prototypens evne til å ta målinger direkte på prøvemateriale ble vurdert.

Det ble vist at bruken av den håndholdte multispektrale bildetakeren direkte på laksefileter ga en signifikant ($p<0.05$) reduksjon av refleksjonen i hele spektret, sammenlignet med billedtakning av 10x10 cm filetportioner lagt i petriskåler. Fargemålinger med multispektralbildetakning ga lysere (L*=59,1±1,0), mer mettet (C*=57,3±1,6) og gulere farge (h*=50,9±0,7) enn et RGB-fargemålingssystem (L*=55,0±1,8, C*=49,5±2,0, h*=43,9±0,5). Det ble vist liten forskjell mellom de to instrumentene når laksefileter ble rangert etter SalmoFan™-fargekort-score med bruk av kromverdier (C*), med en gjennomsnittlig forskjell mellom instrumentene på 0,15 fargekort-score. Det multispektrale instrumentet hadde en tendens til å gi høyere fargekort-score enn det RGB-baserte instrumentet, men den høyeste forskjellen mellom instrumentene var på 1 fargekort-poeng. Måling av melaninflekker ga en signifikant forskjell i refleksjon for alle syv bølgelengdebånd sammenlignet med normal laksefilet-vev spektra som betyr at instrumentet kan enkelt detektere melaninflekker.

Det ble funnet høy korrelasjon mellom multispektral data og QIM-score av hodet-på-sløyet laks lagret på is. 405 nm båndet ga den høyeste negative korrelasjonen (r=-0,792) tatt av buk-skinn-regionen. Gjellene ga en signifikant ($p<0,05$) seperasjon ved 850 nm mellom fersk (dag 1), modnet (dag 8) og forringet (dag 17) prøver og viste en høy positiv korrelasjon (r=0,696) med QIM-score. Det ble også vist høy korrelasjon med bakteriell vekst ved 405 nm spektrumet av lakseskinn for APC (r=-0,625), *Pseudomonas ssp*. (r=-0,744), H_2S-produserende bakterier (r=-0,719) og total aerob psykrotorf platetelling (r=-0,614). Gjeller viste lignende høy korrelasjon (r>0,6) for bakterievekst ved 850 nm spekteret.

Bruken av den multispektrale billedtakningsprototypen direkte på hele laksefileter ga flere variabler som kunne påvirke resultatene, og det førte til økt partiskhet fra operatøren av instrumentert. Det ble foreslått at fremtidige design av prototypen bør minke påvirkningen av disse variablene. Det ble vist at prototypen kunne måle og evaluere fargen av laksefilet på lik stilling som industrielle fargemålingsmetoder og deteksjon av melaninflekker ble oppnådd. Den multispektrale bildetakningsprototypen viste evne til å korrelere spektraldata med mikrobielle og sensoriske metoder for kvalitetskontroll, og har muligheten til å bli et utmerket verktøy for å forutsi kvalitet og holdbarhet av hodet-på-sløyet laks.

Preface

This thesis was written as a part of the MSc programme Food science, technology, and sustainability at the Norwegian University of Science and Technology (NTNU), counting for 45 credits. The work conducted in this thesis collaborated closely with the TraceMyFish research project at NTNU.

I own much gratitude and thanks to those around me for helping med complete this thesis. I would like to thank my supervisors Professor Jørgen Lerfall and Associate Professor Anita N. Jakobsen for their counselling and guidance. A special thanks to my research associates Jørn-Owe Johansen and Sine Marie Moen Kobbenes for their invaluable help with lab and data processing work. I would also like to thank engineer John-Kristian Jameson, PhD candidate Sophie Kendler, and engineer Martin Haider for their help with analyses in the lab.

Lastly, I want to thank my friends and family for all their support through five years of study and for always being there when I need you.

_____

Trondheim May 29th 2023

Marcus Hoff Hansen

Table of Contents

List of Figures

List of Tables

List of Abbreviations

ADP	Adenosine Diphosphate
ANOVA	Analysis of Variance
ATP	Adenosine Triphosphate
C*	Chroma
Ca^{2+}	Calcium ion
CIE	International Commission on Illumination
DHA	Docosahexaenoic Acid
EPA	Eicosapentaenoic Acid
h*	Hue
H_2S	Hydrogen Sulphide
HOG	Head-on-Gutted
HPLC	High Performance Liquid Chromatography
HSI	Hyperspectral Imaging
L&H	Long and Hammer
L*	Lightness
LCh	Lightness, Chroma, and hue
LED	Light-Emitting Diode
MAP	Modified Atmosphere Packed
MRS	De Man, Rogosa and Sharp agar
MSI	Multispectral Imaging
nCDA	Normalized Canonical Discriminant Analysis
NIR	Near infrared
NQC	Norwegian Quality Cut
NTNU	The Norwegian University of Science and Technology
QIM	Quality Index Method
RGB	Red, Green, and Blue
SSO	Specific Spoilage Organism
TMA	Trimethylamine
TMAO	Trimethylamine N-oxide
VM	Videometer

1 Introduction

The Atlantic salmon *(Salmo Salar L.*) is a species of the salmonid family and is commonly found in areas around the north Atlantic. Since the 1970's the farming of Atlantic salmon has become a significant industry for coastal areas around and outside the north Atlantic. Norway alone produced 1 364 044 metric tons of salmon in 2020, and the demand for salmon is increasing globally (Kidane & Brækkan, 2021; SSB, 2020).

Salmon is a high-quality food source containing important macronutrients such as proteins and lipids, as well as micronutrients like vitamins and minerals (FAO/WHO, 2011; Hicks et al., 2019). Salmon is an oily fish that provides essential long-chain omega-3 polyunsaturated fatty acids (PUFA) such as eicosapentaenoic acid (EPA) and docosahexaenoic acid (DHA). These fatty acids are believed to help brain and eye development in children and have shown to reduce the risk of heart and cardiovascular diseases (Mozaffarian & Wu, 2011; Stonehouse, 2014), though the evidence is not conclusive in all cases (Manson et al., 2018). Salmonids stores fat in the muscle tissue and connective tissue, unlike lean fish such as cod and other white fish which stores fat in the liver (Nanton et al., 2007; Polvi & Ackman, 1992).

Farmed Atlantic salmon is also regarded as parasite free, meaning that parasites that cause disease in humans such as the nematode *Anisakis* are absent in farmed salmon (Lunestad, 2003). This fact helped establish consumption of raw and mildly treated salmon products form Norwegian aquaculture to the global marked (Odden, 2020). Raw salmon products have high requirements in terms of quality and food safety that requires extensive quality testing throughout the value chain of farmed Atlantic salmon (Lerfall et al., 2023). Established methods for quality testing of salmon are often time consuming, laborious, and destructive (Cheng et al., 2013). In recent years, non-destructive methods for quality monitoring of food have emerged, and shown promising results in predicting chemometric and microbial quality parameters (ElMasry et al., 2011; Jiang et al., 2023). Multispectral and hyperspectral imaging is an increasingly popular non-destructive method, giving fast accurate results based on spatial and spectral data which can

be used to monitor product quality throughout the entire value chain of a food product (Dissing et al., 2011; Liu et al., 2016; Qin et al., 2013).

Current methods of determining food quality and safety require chemicals and materials that often are toxic and expensive (Qin et al., 2013). Multispectral imaging technology can contribute to a reduction of chemical use and provide a simple, safe and cheap method for the determination of food quality (Schultz et al., 2023). It can also contribute to safer and better food quality in the developing world, especially within fishery and aquaculture food sector which has one of the greatest potential for being a sustainable food source for the worlds growing population (FAO, 2022).

1.1.1 The atlantic salmon value chain

To be able to identify where to apply the potential for non-destructive technology is important to map the stakeholders concerns and interest within a defined value chain. The Norwegian Atlantic salmon value chain is defined as the product flow following the path from farming to the end consumer. The product will go through several steps in the value chain and these main steps are Farming, harvesting, processing, retailing, and finally the end consumers. From Norway around 80% of the total production of farmed salmon is exported as whole head on gutted (HOG) fish that is packed in Styrofoam boxes and transported by trucks to secondary processors or wholesale/retail markets (Lerfall et al., 2023).

Around 80% of the total production goes to the EU and around 13% goes to the Asian markets, EU being the largest market for Norwegian farmed salmon. Most the market supply to the EU is fillets (~47%), smoked salmon (~28%), whole (~12%), and the remaining 13% are of other value-added products (VAP). The last VAP are dominated by conveniency products such as ready-to-eat and ready-to-heat types of products (Lerfall et al., 2023).

1.1.2 TraceMyFish

This MSc thesis collaborated closely with the TraceMyFish research project and is founded by the ERA-NET BlueBio Cofund initiative, and its full title is “Traceability and Quality Monitoring throughout the Fish Value Chain”. The projects goals are to design and implement the inteligentFishManagementSystem (iFMS) that can

track and trace safety and quality-critical information over the targeted value chains. It will establish a data infrastructure that can collect, pre-process, and analyse data coming from new portable sensing devices like spectral imaging. That can inform specialized AI models and architecture that gives risk prediction to different actors in the value chain (TMF, N.D.).

TraceMyFish bring together research and industrial partners with expertise in different scientific and technical disciplines that is critical for the project. These partners are SCiO, AUA, NTNU, Videometer A/S, University of Iceland, and Matis Food and Biotech R&D.

1.2 Causes for loss of freshness and spoilage in raw salmon-products

Quality is often defined as consumer acceptance, though this is a troublesome term as quality for the consumer will vary between every individual. Industrial stakeholders will also have a different understanding of quality than the consumer. Industrial actor in the food industry is more concerned for parameters such as food safety and nutritional composition. Consumers on the other hand will evaluate quality mainly based on organoleptic parameters such as appearance, odour, and taste. In the case of seafood, freshness is parameter that is important to both industry and consumers, due to the highly perishable nature of seafood (Komolka et al., 2020).

Quality and quality changes in fish can be categorised in different stages based on the cause of the change. Huss (1976) made a graph illustrating the changes in quality of fish stored on ice over time seen in Figure 1-1. The graph also shows forces affecting the quality degradation of the fish, where autolytic forces are the main contributor at the start. After a few days the bacterial activity takes over as the main contributing factor to the degradation of quality. In this example the fish will be spoiled and rejected as edible after 12 days on ice.

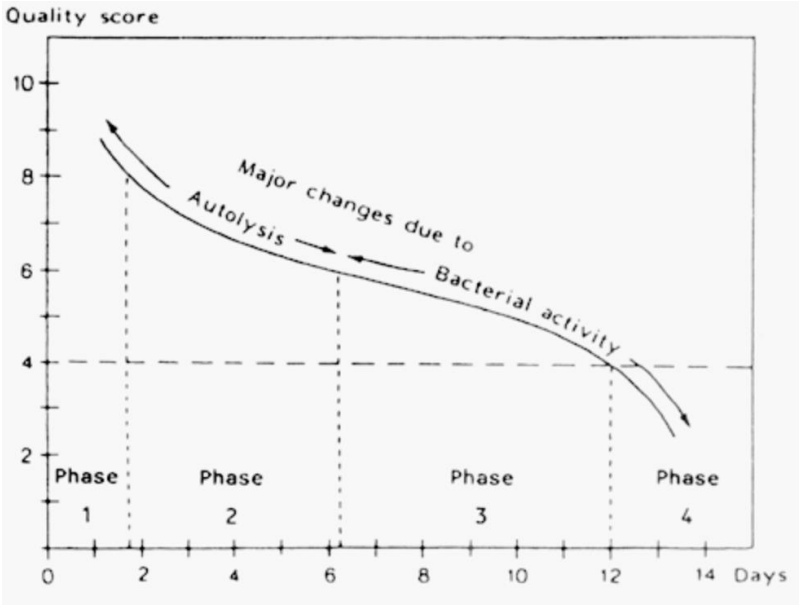

Figure 1-1 A graph showing the quality changes of fish (cod) stored on ice and the forces that causes them (Huss, 1976).

1.2.1 Salmon muscle composition and quality changes

The muscle is the most abundant tissue in salmon, making up for around 65% of the total body mass (Weatherley et al., 1979). Aquatic animals like fish don't have muscles that connects with the skeleton like terrestrial animals. Instead, the muscle cells are arranged in parallels and connected to sheets of connective tissue called myocommata, which are again connected to the skeleton and skin (Huss, 1995). Bundles of parallel muscle cells are called myotomes. The muscles are arranged in two fillets that is situated on the ventral sides of the fish. Each myotome is oriented in the longitudinal direction of the fish and is connected between two myocommata sheets running in the horizontal direction (Altringham & Ellerby, 1999). For salmonoids the myotomes can be seen in the fillet laying in tilted w-shaped segments as seen in Figure 1-2.

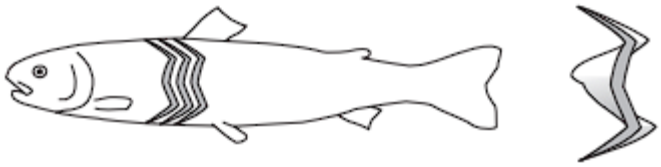

Figure 1-2 Shows the myotomal structure of teleost (incl. salmonids) fish. An isolated myotome is showed on the right side (Altringham & Ellerby, 1999).

The myotome is made up of many muscle cells which are the functional unit of the muscle, responsible for muscle contraction. Each muscle cell is made up of the proteins myosin, actin, tropomyosin and troponin that again makes the functional myofibril proteins responsible for muscle contraction (Huss, 1995; Ojima, 2019). Myosin makes up about 50% of muscle proteins while actin makes up for around 25% (Sotelo et al., 2000). As seen in Figure 1-3 the two proteins in the myofibril are shaped as long parallel bundles of threads, where the thinner actin filament is fastened to a horizontal z-shaped line called the z-disc (Ojima, 2019). The area between each opposite laying is called a sarcomere and the between each row of actin filament that lays horizontally is the myosin filament. The myosin is not connected to the z-line directly, but it is connected to an elastic filament called titin and is also able to contract the muscle by temporarily connecting to the actin filament and pulling along it (Cooper, 2000).

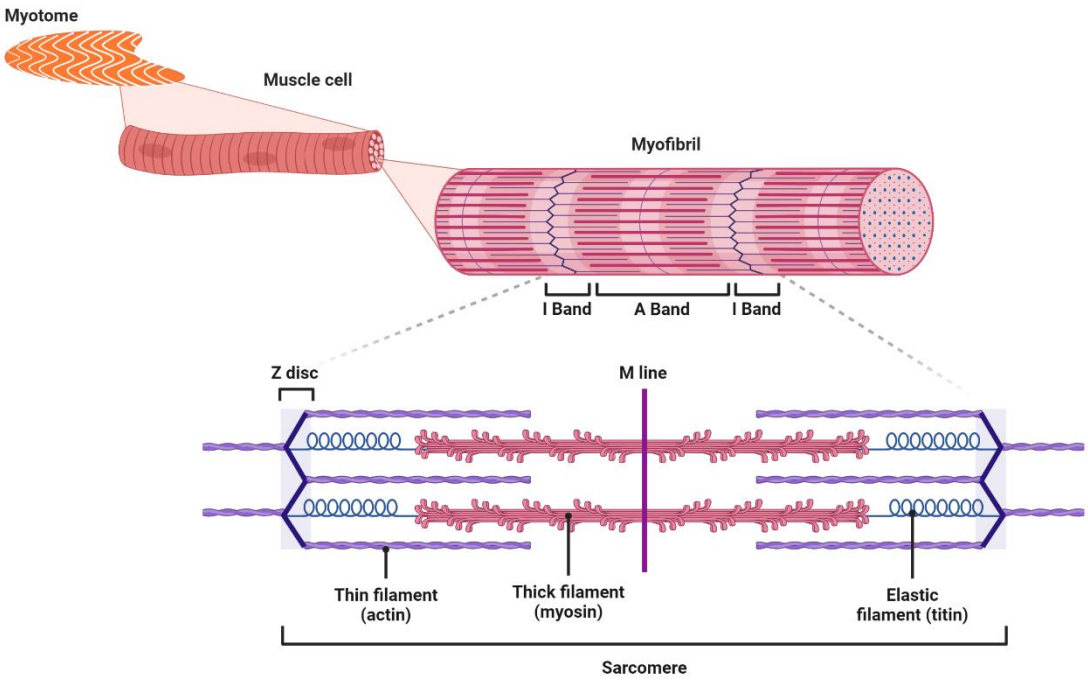

Figure 1-3 Shows the structure of the structure of the muscle from a fillet down to a single sarcomere. The figure was made with BioRender based on Ojima (2019).

The exact process of muscle contraction starts with a nerve impulse that alters the permeability of the muscle cell membrane called the sarcoplasmic reticulum. Ca^{2+} ions are then able to enter the myofibrils which activates enzymes in the myosin "head" that split ATP to ADP with the help of creatinine. At the same time Ca^{2+}

makes troponin on the actin filament reciprocate making an available spot for the myosin to connect (Hannisdal & Hemmer, 2017; Hemmer, 1997). The release of ADP and phosphorus form the head of the myosin connected to the actin will release energy, and the myosin head will change angle. The motion results in the actin filament being pulled towards the middle of the sarcomere. ATP will then connect to the myosin head and release the connection between the myosin and actin filament. The cycle is started again when ATP is split to ADP and phosphorous and will continue as long there is Ca^{2+} ions and ATP. Every time the cycle repeats itself the myosin head will move one step further along the actin chain leading to the contraction of the muscle. The muscle will only relax when the nerve impulse stops, and calcium ions is pumped out of the muscle cell (Hannisdal & Hemmer, 2017).

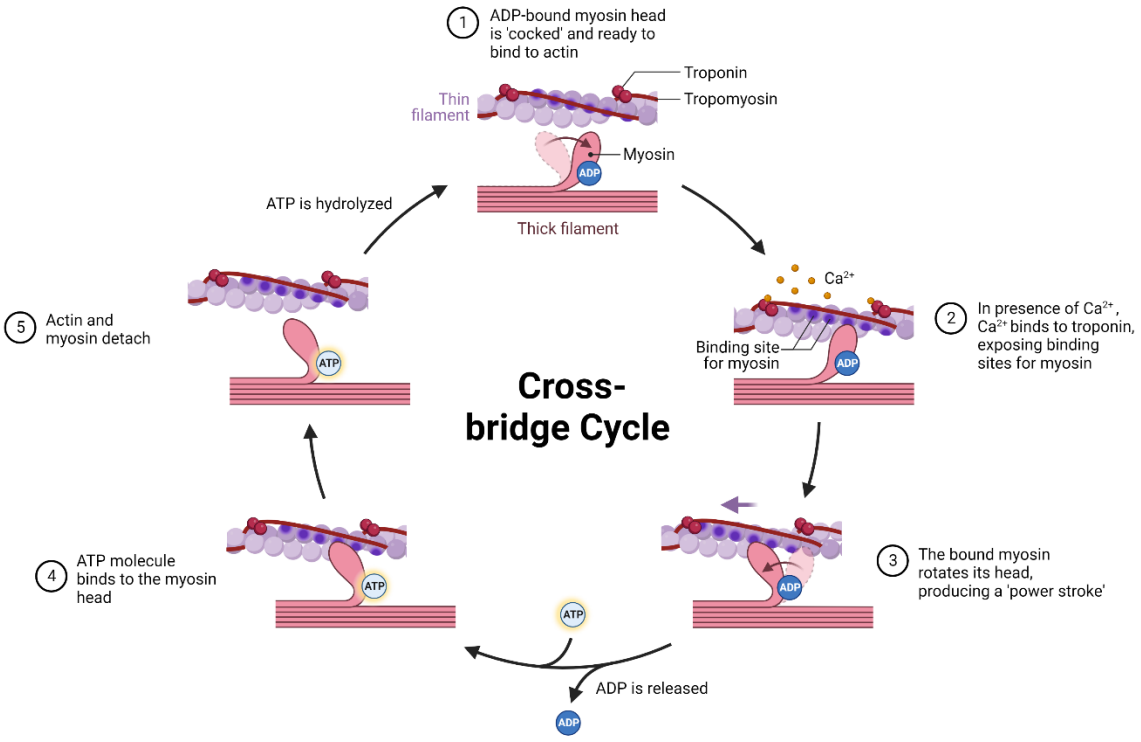

Figure 1-4 Illustrates the crossbridge cycle and shows how muscle contraction occur by the interactions of myosin, actin, ATP, and other components. The figure was created with biorender.com based on (Kim, 2021).

Healthy fish metabolises energy for muscle contraction through several pathways. The most common pathway is through glycogen from stored carbohydrates or lipids (Harmon et al., 2011; Karatas, 2018). The glycogen is broken down to glucose which are again reduced to ATP and pyruvate. Pyruvate can be

metabolised aerobically and anaerobically, the first giving significantly more energy through the TCA cycle with 36 moles of ATP for each mole of glucose, The latter can only produce two moles of ATP comparatively (Hemmer, 1997). In living fish, the aerobic metabolic pathway will always be chosen as long oxygen is available. However, at the point of death the supply of oxygen is stopped due to oxygenated blood from the gills are no circulated by the heart, and thus not delivered to the muscle cells (Huss, 1995). The lack of oxygen leads to anaerobic glycolysis being the main pathway for ATP production. ATP can also come from small reserves of creatine phosphate and ADP, but it is rapidly depleted in only a few minutes after death. Remaining glycogen in the muscle is broken down by enzymes into ATP and lactic acid through a range of phosphorylated sugar derivatives. The production of ATP in the muscle is finally stopped either by substrate depletion (glycogen), or the inhibition of glycogenic enzymes due to pH reduction from lactic acid accumulation in the muscle (Daskalova, 2019).

Soon after the point of death the concentration of calcium ions in the muscle cells sarcoplasm will increase. ATP is needed for the calcium pump to regulate the levels of Ca^{2+} in the muscle cell, and when the supply of ATP drops down below a certain level the calcium pump is no longer able to pump Ca^{2+} back out the sarcoplasmic reticulum. The inability to regulate calcium ions results in an uncontrolled muscle contraction called rigor mortis (Hannisdal & Hemmer, 2017).

1.2.2 Proteolytic changes

The muscle tissue that is in a state of rigor mortis will soften which is related to the activation of proteolytic enzymes in the muscle cell (Huss, 1995). The proteases cathepsins are believed to contribute to autolytic degradation of fish muscle tissue. Cathepsins are proteases with a low pH range of activity usually found in the muscle cells organelles called lysozomes (Reddi et al., 1972). For salmon it is believed that cathepsin L is the most active enzyme in fish muscle degradation, and it is shown that it can break up both myofibrillar proteins and connective tissue (Yamashita & Konagaya, 1990). Calpains is another group of proteases associated with the tenderisation of flesh. Functionally calpains are responsible for autolysis of the z-line proteins of myofibril which impacts the texture of the muscle (Geesink et al., 2006). The softening of the fillet flesh

through autolysis is a serious concern and limits the commercial value (Koteng, 1992).

1.2.3 Bacterial activity

Spoilage of fresh fish are mainly due to bacterial growth. Bacteria exists naturally on the outer surface of fish and are also found in gills and intestines. The flesh is normally sterile as the active immune system prevents bacterial growth. When the fish dies the immune system collapses, allowing for bacteria to grow on exposed flesh. The growth of bacteria depends on extrinsic and intrinsic factors such as water content, pH, temperature, and processing. These factors also play a part on the species of bacteria that can grow forth on the substrate. The microbial quality of fish is dependent on the present microorganisms spoilage potential and the conditions that affect the growth and formation of spoilage metabolites (Gram & Huss, 1996).

The most common species that is found on chilled aerobically stored salmon are species within the genera *Pseudomonas (P.), Shewanella (S.)* and *Photobacterium (Ph.) phosphoreum,* The latter being more dominant in CO_2 rich environments which is relevant for modified atmosphere packed (MAP) fish (Emborg et al., 2002; Gram & Huss, 1996; Parlapani & Boziaris, 2016; Tryfinopoulou et al., 2002; Xie et al., 2018). It is documented that live salmon harbours subspecies of these bacteria and is therefore considered the primary source of spoilage organisms on processed salmon (Cantas et al., 2011; Gram & Huss, 2000; Hovda et al., 2012; Møretrø et al., 2016).

Spoilage is not necessarily connected to bacterial counts, but rather to the amount of metabolic spoilage products caused by specific spoilage organisms (SSO) (Fogarty et al., 2019). The most important spoilage products are H_2S and reduction of trimethylamine oxide (TMAO) to trimethylamine (TMA), and is responsible for the smell commonly associated with spoiled fish(Sveinsdottir et al., 2002).

1.3 Current quality assessment methods for salmon

1.3.1 Colour assesment

The distinct orange colour of the salmon flesh comes from the deposition of the pigment carotenoid astaxanthin in the flesh (Torrissen, 1989). Salmonids does not have the ability to biosynthesise astaxanthin but acquires it through feed. In the wild, salmon acquires carotenoids from microcrustaceans such as krill. Farmed salmon does not eat live food and synthetic astaxanthin and/or other carotenoids are added to the feed (Viera et al., 2018). The colour pigment is absorbed through the intestinal tract and deposited in the flesh (Matthews et al., 2006), but only 40-60% of ingested pigment is absorbed through the gut and only 10% are deposited into the flesh (Bjerkeng et al., 2007; Ytrestøyl et al., 2006). This has led to increasing amount of astaxanthin added to the feed to achieve better colouration of the salmon fillets and amounts have doubled since 2000 (Aas et al., 2022). Astaxanthin is estimated to make up for 15-25% of the total feed costs (Amoroso et al., 2020), and recent reports show that the colouration of salmon fillets have decreased despite increased levels of pigment in the feed (Ytrestøyl et al., 2019). This poses a major challenge for the aquaculture industry since colour intensity is linked to the amount costumers are willing to pay for the product (Alfnes et al., 2006; Torrissen et al., 1988). The importance of controlling the colour of salmon fillets within the industry is apparent and good oversight could help detect changes in colour quality as new practises are applied.

Since colour is an important quality criterion, the aquaculture industry has adopted several methods of measuring the colour value of fillet flesh (Anderson, 2000). The standardized method of colour grading in the Norwegian salmon farming industry is by using the DSM SalmoFan™ colour card fan. SalmoFan™ has a set of numerated colour cards that is used to compare and grade salmon fillet colour (Skrede et al., 1990). The values of the SalmoFan™ cards range from 20-34 and commercial actors have a goal to lay in between the range of 27 to 29 (Anderson, 2000). The SalmoFan™ is an improvement over the former Roche colour cards, and the colour of the cards is based on different saturation levels of the colour pigment astaxanthin. The SalmoFan™ colour score has been shown to have a positive correlation with total pigment concentration, however pigment concentration may not be the only factor that is that is important for colour

perception (Johnston et al., 2006; Torrissen et al., 1995). Factor such as actomyosin content, muscle fibre density and pigment type in the flesh may also play important roles in the perceived colour of salmon flesh (Johnston et al., 2000; Johnston et al., 2006).

Instrumental colour measurements done with red, green, blue (RGB) cameras or other colourimeters are frequently used in research to determine colour values of salmon fillets (Erikson & Misimi, 2008; Lerfall et al., 2016; Yesilayer, 2020). The extracted values are normally based on the International Commission on Illumination's (CIE) tristimulus values. The three values are described as lightness (L*) that is the ratio between dark (0) and light (100), The relation between red and green (a*), and the relation of yellow and blue (b*). Together these values are used as coordinates (x, y, z) in a three-dimensional colour map to point out a specific colour. Additionally, the CIE L*, a*, and b* can be calculated into chroma (C*) which defines the saturation of colour, and hue angle (h*) that can be described as the angle in a colour wheel defining the colour (CIE, 2004).

1.3.2 Melanin

Melanin is a term commonly used to describe a black pigment of biological origin, but in the salmon industry it is used to describe the appearance of dark pigmented spots in salmon fillets. These spots are usually around 2-3 cm wide but can be larger and appear mostly in the forward abdominal area under the ribs (Mørkøre, 2017). The cause for the appearance of melanin spots is not known however factors such as water conditions, health condition, mechanical injuries, sexual maturity, and feed can impact the development of melanin spots. What is known is that melanin is synthesized by enzymes in melanin containing cells called melanomacrophages, and that these cells express the melanin synthesising gene during chronic inflammation of Atlantic salmon (Hossain, 2022; Mackintosh, 2001).

Melanin spots in salmon fillets are seen as a defect and consumers do not prefer to buy spotted fillets. This has led the salmon processing industries to cut away defect parts of the fillet or discarding the whole fillet in some cases (Hossain, 2022). The salmon industry have expressed interest in sensor systems that can detect melanin and is able to trace the effected part over the value chain down to the specific package (Lerfall et al., 2023).

1.3.3 Quality Index Method

As previously mentioned, fish is susceptible to various changes post-mortem that affect the overall quality of the product. The knowledge of the various descriptors associated with the spoilage process allows us to evaluate the optimal condition of the product and its ability to retain those characteristics over time (Freitas et al., 2021). Collecting this information allows for the estimation of the time that has elapsed since slaughter and helps estimate the time of rejection for consumption. Sensory analyses are a useful tool for collecting this information, since the sensory clues are parameters that the consumers can understand and follow when purchasing fresh fish. Sensory evaluations can be performed at different levels of the seafood industry and are usually performed at the processing plant or auction sites (Freitas et al., 2021), but are also used for research.

The quality index method (QIM) is one of the most frequently used methods for evaluating freshness of fish stored on ice. The method was originally developed by the Tasmanian food research unit as a rapid way to assess fish freshness (Bremner, 1985). The method was adapted for assessment of head-on-gutted salmon by Sveinsdottir et al. (2002), and uses quality attributes for appearance/texture, eyes, gills, skin, abdomen and description of how these change with storage time. The use of QIM is however, limited by sampling size, storage conditions, and assessors experience which makes it a subjective method (Bernardo et al., 2020).

1.4 Spectral imaging

Spectral imaging is the results of combining traditional imaging with spectroscopy to combine spectral and spatial data into one. Normally it is not possible to acquire spectral data from traditional RGB imaging and spectroscopy cannot cover large sample areas. The combination of these provides both spatial and spectral information of the target, which makes it a very useful tool for evaluating food items. There has been a rapid development of the technology over the past decade and has provoked a high interest from both industrial and academic areas.

Spectral images can be described as a three-dimensional image since it contains two spatial dimensions (x & y) and one spectral dimension (λ). Ordinary RGB imaging cameras also captures spectral information, though its only by three

broadband colour channels that produces a single colour value for each pixel (ElMasry et al., 2019). Spectral imaging distinguishes itself from RGB imaging since it can capture multiple discrete wavelengths resulting in a higher spectral resolution than RGB imaging. This is very useful in cases of the phenomenon called metamerism, that is when samples which are visually perceived as similar in colour, but has spectral variation within a single broadband range (Setchell, 2012).

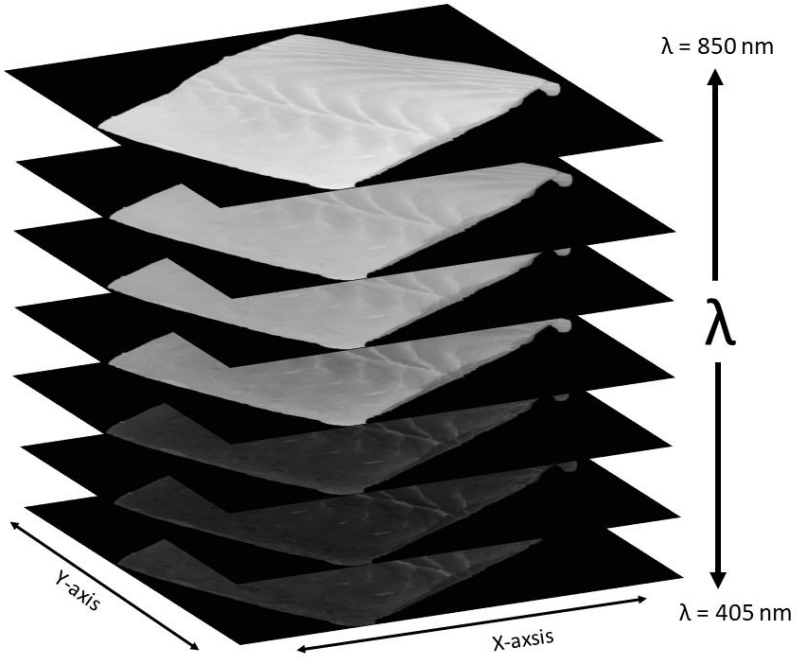

Figure 1-5 Visualizes the three-dimensional image taken from a multispectral device, where the special dimensions are represented by x and y and the spectral dimension is represented by λ.

Depending on the continuity and broadness of the wavelengths in the spectral dimension, we can divide spectral imaging into two techniques: Multispectral imaging and hyperspectral imaging. The multispectral imaging (MSI) technique acquires a few discrete wavebands, while the hyperspectral imaging (HSI) technique can acquire up to tens or hundreds of continuous wavebands. This means that for the multispectral images each pixel contains isolated datapoints of spectral data due to the separate wavelengths taken. The hyperspectral images however contain a full spectrum in each pixel. There are up and downsides for both techniques, Primarily the number of wavelengths that image contains and the data size of each image. Hyperspectral imaging gives much higher spectral resolution often down to 1 nm between each band; however, this increases the size of the image data as well and poses a challenge in data logistics. Multispectral imaging on the other hand has smaller data files and are thus much simpler and can be

handled by modern commercial computers, making it more practical for situation where high spectral resolution is not required (Qin et al., 2013).

Various techniques can be used for capturing multispectral imaging. The most common of these techniques are line scanning, point scanning and area scanning. The use of these is dependent on the application the instrument will be used for. Line scanning for example is best suited to scan products moving on a conveyor belt as the name implies the instrument only scans one spatial dimension at a time. Area scanning can scan the entire spatial dimension in one image but needs to take several images to get spectral information (Qin et al., 2013).

1.4.1 Videometer multispectral imaging

Videometer AS was responsible for developing a multispectral imaging device that is easy to use, cost-efficient, and portable for the use in traceability, safety and quality of seafood products (Schultz et al., 2023). This development led to the handheld MSI prototype device called VideometerLite shown in Figure 1-6.

Figure 1-6 The VideometerLite multispectral imaging prototype (Schultz et al., 2023).

The VideometerLite is based on Videometer's spectral imaging technology where multispectral images are achieved by using an integrating sphere with a camera placed at the top, LEDs of different wavelengths are situated around the equator of the device. The integrating sphere is hollow, and the inside is covered by a reflective coating that ensures a uniform light scattering and diffusion effects form the light of the LEDs. MSI is taken by the area scan method and uses sequential

LED strobing to capture stacks of images at different wavelengths (Carstensen & Flom-Hansen, 2006; Schultz et al., 2023).

The VideometerLite has an integrating sphere of 130 mm and can capture images in seven different wavelengths within the spectrum of 405-850 nm, these being 405 nm, 460 nm, 525 nm, 590 nm, 621 nm, 660 nm, and 850 nm. The wavelengths were chosen due to their cost to efficiency ratio, having a sufficient cover of the visible range (VIS) and the inclusion of ultra violet (UV) and near infrared (NIR) wavelengths (Schultz et al., 2023).

2 Aims of the thesis

This thesis goals was closely coordinated with the TraceMyFish goals of the Atlantic salmon value chain in work package 6 "*Piloting and evaluation"*, defined by Nychas et al. (2023). The background for this thesis goals is based on the results from interviews of Norwegian enterprises within the Norwegian Atlantic Salmon value chain, conducted by Lerfall et al. (2023). Based on this information this thesis main objective was stated as following: To test and evaluate the handheld multispectral imaging prototype "VideometerLite" abilities in measuring physiochemical, sensory, and microbial quality parameters of raw and mildly processed Atlantic salmon. Within the main objective of this thesis, three sub-objectives were defined.

1. To assess the MSI prototype's ability to measure colour properties of Atlantic salmon fillets.
2. Investigate the possibility to detect melanin-spots with multispectral imaging.
3. Asses the feasibility of using multispectral imaging to detect changes in freshness and spoilage of head-on-gutted salmon stored on ice.

3 Materials and Methods

3.1 Chemicals

The chemicals used in this thesis are listed in Table 3-1. All chemicals used are of analytical grade, unless specified otherwise.

Table 3-1 List of chemicals and chemical products used.

Chemical name/Product name	**CAS-number/Article number**	**Producer/supplier**
Acetone, HiPerSolv CHROMANORM®	CAS:67-64-1	VWR
Agar	CAS: 9002-18-0	VWR
Ammonium iron(III) citrate	CAS: 1185-57-5	Merck
Astaxanthin	CAS:7542-45-2	Merck
Chloroform, AnalaR NORMAPUR®	CAS:67-66-3	VWR
di-Potassium hydrogen phosphate	CAS: 7758-11-4	Merck
Gelatine	CAS: 9000-70-8	Thermo Fisher
Hexane, HiPerSolv CHROMANORM®	CAS:92112-69-1	VWR
L-Cystein	CAS: 52-90-4	Merck
Methanol, HiPerSolv CHROMANORM®	CAS:67-56-1	VWR
MRS AGAR	ArtNo. 84607.0500	VWR
PROTEOSE PEPTONE	CAS: 91079-46-8	Thermo Fisher
Pseudomonas Agar Base	ArtNo. CM0559	Thermo Fisher
Pseudomonas CFC Selective Supplement	ArtNo. SR0103	Thermo Fisher
Sodium chloride, AnalaR NORMAPUR®	CAS:7647-14-5	VWR
Sodium thiosulphate	CAS: 7772-98-7	Thermo Fisher
Sodium thiosulphate	CAS: 7772-98-7	Thermo Fisher
Yeast Extract Powder	CAS: 8013-01-2	Thermo Fisher

3.2 Experimental design

In this thesis a multispectral imaging prototype was assessed in its ability to measure colour and melanin-spots of salmon fillets and detecting freshness and spoilage of head-on-gutted salmon. The prototype was tested against conventional methods for measuring these parameters. Figure 3-1 shows the experimental design of the entire thesis with the included analysis.

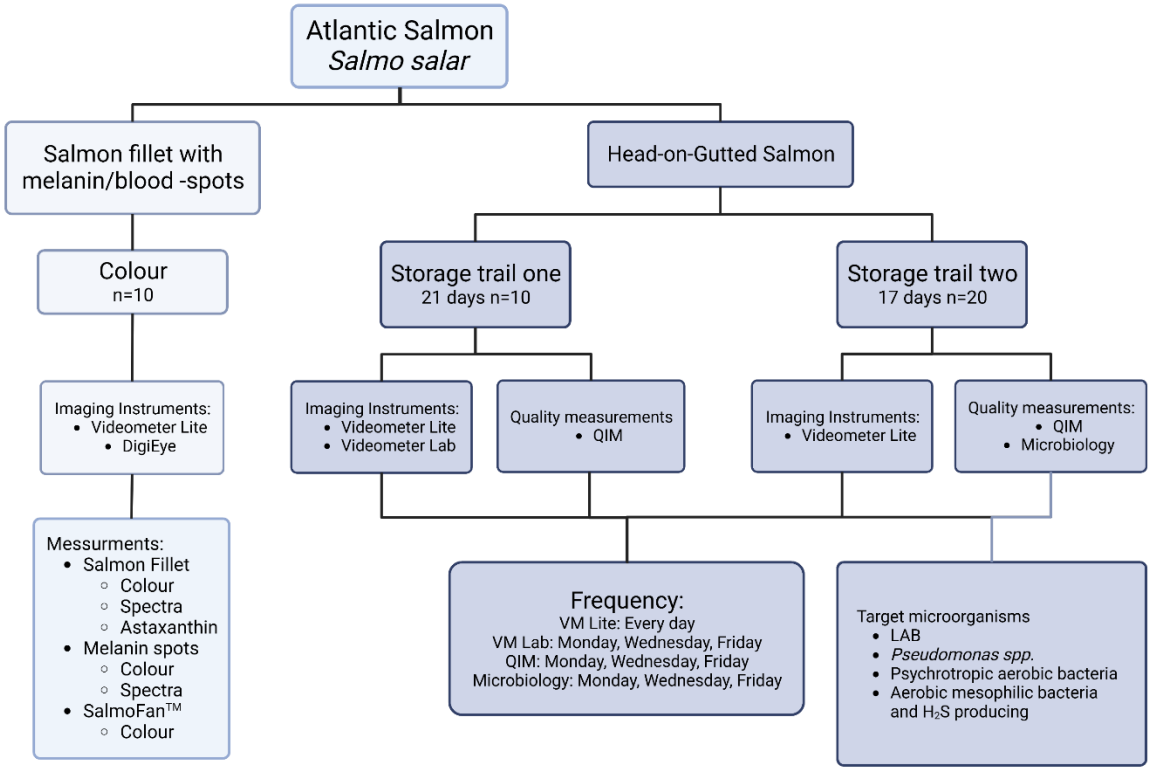

Figure 3-1 Illustration of the entire project experimental setup. Two different sample materials were used which was salmon fillets containing melanin and bloodspots and head on gutted salmon. Three separate experiments were performed where the first was measurements of colour and melanin in salmon fillets. The second experiment was a storage trail of head-on-gutted salmon where VM Lite was tested in detection for loss of freshness with the use of sensory methods as reference. The last experiment (storage trail two) was a replication of the second with additional measurements of microbial growth.

3.3 Image protocol assesment

The mobile nature of the VideometerLite multispectral imager makes it possible to take multispectral images directly on the sample surface, without cutting the sample into a shape that fits inside the opening of the integrating sphere. To validate this imaging protocol, it was tested against a control protocol. The control protocol used salmon fillet samples that were cut to fit inside a standard petri dish. The samples where then placed on a white cutting board and the VideometerLite was placed over the sample for imaging as seen in Figure 3-2 Shows how the

Figure 3-2 Shows how the samples was prepared for the controlled image protocol.

samples was prepared for the controlled image protocol.

The direct imaging protocol was done by placing the VideometerLite instrument directly on the region of interest on the salmon fillet sample. Both protocols were used on all experiments with salmon fillet samples. Only the direct imaging protocol was used in the storage trail experiments.

3.4 Flesh colour assessment

The Salmon fillets was obtained from Lerøy AS. A total of 20 fillets was used and all fillets had visible melanin or blood-spots. The fillets contained top loin, loin, skin, and pin-bones. The instruments used for colour measurement was VideometerLite multispectral imaging system (Videometer A/S, Herlev, Denmark),

and DigiEye digital colour measurement system (DigiEye full system, VeriVide Ltd, UK) with a connected camera (Nikon D90, 35mm lens, Nikon Corp., Japan). Images taken with the DigiEye instrument was done by placing whole fillets on a white cutting board and moving them inside the lightbox (Verivide daylight, 6400 k, UK) with the D65 illuminant setting applied. Images taken with VideometerLite instrument for colour measurement of salmon fillets used the NQC region of the samples and both imaging protocols was applied.

As a standard colour reference for salmon flesh, the SalmoFan™ (Hoffman-La Roche, Basel, Switzerland) colour grading cards was imaged with DigiEye and VideometerLite using the colour gradient-score numbered 20 to 34 of the SalmoFan™. The extracted chroma values (C*) was observed to give the best difference between SalmoFan™ gradients. This value was then chosen to score the salmon fillet samples by matching chroma-values of the fillets to the closet matching SalmoFan™-card's chroma value.

Analysis of the Digieye images was done with the DigiProduction software version 3.1.2.6 (VeriVide Ltd., UK) by selecting the NQC-region of the fillet with a rectangle selecting tool and extracting the mean L*, a*, b*, C*, and h* values from the selected region of interest. The VMLite images was processed with the VideometerLab software version 13193 (Videometer A/S, Herlev, Denmark), where segmentations excluding background and connective tissue was applied on the images of the NQC-region. The mean L*, a*, b*, C*, h* and spectral band reflectance values with standard deviations was extracted from the segmented images.

3.4.1 Astaxanthin extraction

20 10x10 cm fillet samples from the NQC-region were used for Astaxanthin extraction. The samples came from the previous colour imaging trial and was frozen and vacuum-packed. A modified version of Bligh and Dyer (1959) method for total lipid extraction was used for extracting lipids, that includes the fat-soluble pigment astaxanthin. Preparation of samples was done by grating the frozen fillet samples and weighing about 3 grams of the grated material on an analytical weight, noting the exact weight. The weighted samples were then placed in marked centrifuge tubes. Each tube received the following treatment:

1. Addition of 3.0 ml deionized water, 10.0 ml Methanol and 5.0 ml Chloroform
2. Homogenisation with Ultra Turrax (IKA T25 Digital) 1700 rpm for 1 minute
3. Addition of 5.0 ml of Chloroform
4. Homogenisation for 20 seconds
5. Addition of 5.0 ml of deionized water
6. Homogenisation for 20 seconds
7. Centrifugation at 10 000 g for 10 minutes

After centrifugation the content of the tubes had separated into three phases with methanol/water-phase at the top, solid-phase in the middle and chloroform-phase at the bottom. The chloroform-phase was extracted using a glass Pasteur pipette and transferred to a new centrifuge tube. Afterwards 3 ml of the chloroform-phase was transferred to a weighted klimax tube. The klimax tubes was then transferred to an evaporator with nitrogen gas and temperature set at 50°C. The samples were left to evaporate for approximate 15 minutes until the chloroform had evaporated out of the samples.

The remaining lipid fraction was then analysed by high-performance liquid chromatography (HPLC), using an Agilent1100 liquid chromatograph (Agilent Technologies, Paolo Alto, CA, USA) connected to an Agilent photodiode array UV-VIS detector. Astaxanthin content was analysed after the method of Vecchi et al. (1987) using a Lichrosorb SI60-5, 125 x 4.0 mm, 5 µm, (Hichrom, Reading, UK) HPLC column modified with orthophosphoric acid (0.1% in CH3OH).

3.4.2 Melanin detection assesment

For imaging of melanin on salmon fillets the VideometerLite instrument was used by placing it on the area of the fillet where the melanin-spots were present. 12 of the 20 fillets supplied was classified as melanin-spots and used measuring the mean melanin spectra. Control imaging protocol was also applied by cutting a 10x10 cm square around the melanin-spot and placing it in a petri dish for imaging.

3.5 Storage trail experiment one

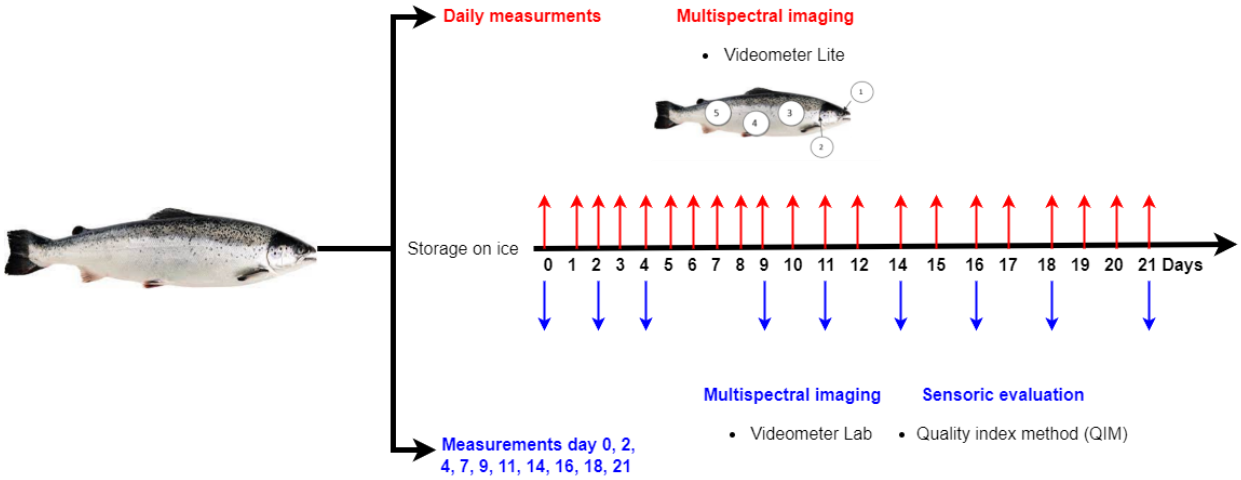

Figure 3-3 Shows the experimental setup for storage experiment one. Red markers show the measurement that was done daily which was imaging with VM Lite. Blue markers show measurements that was done on designated days which were day 0, 2, 4, 7, 9, 11, 14, 16, 18, 21. Imaging with VM Lab2 and sensory evaluations with the QIM-method was done on these days.

A total of 10 head-on gutted (HOG) salmons of superior quality from Lerøy AS was used for the experiment. The fish had been slaughtered the day before the start of the experiment and was bled by a knife stab to the gills. Pairs of HOG-salmon was placed in standard Styrofoam (EPS) delivery boxes filled half-full of ice and with holes on the bottom sides to allow for drainage. Samples was stored in a room fridge at 4ºC outside of measurements and ice was refilled as needed.

Two spectral imaging devices was used during the experiment, which was Videometer Lab2 (Videometer A/S, Herlev, Denmark), a stationary MSI device with 18 separate wavelengths and the Videometer Lite handheld prototype MSI device. The VM Lab2 data was used to compare results with VM Lite to evaluate the handheld prototype performance against a more established MSI device such as the VM Lab2. Spectral imaging was taken with Videometer Lite each day and with Videometer Lab every other working day, meaning Monday, Wednesday, and Friday for 22 days and referring the first day as day 0.

Five distinct imaging zones on the salmon's side profile was identified, based on the QIM-score index, and shown in Appendix 1a. Imaging of eyes and skin regions (eyes, neck, abdomen, and tail) was done every day on both sides of each fish. Imaging of the gills was done on the same days as QIM-measurements by cutting the gill lid open. Figure 3-4 illustrates where the images was captured on each side of the samples.

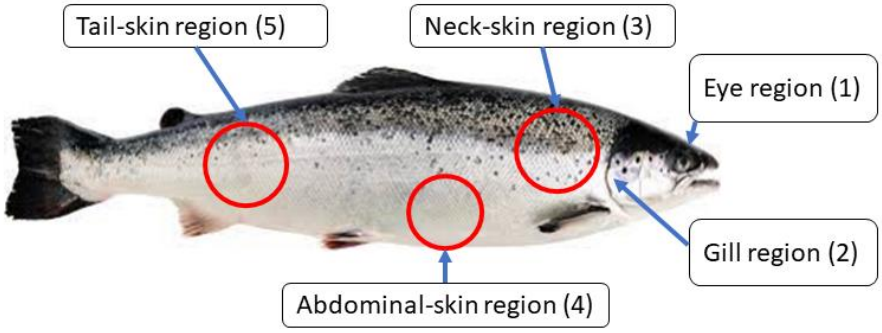

Figure 3-4 The different regions that HOG-salmon samples were imaged by MSI instruments. In total there were five regions on each side of the HOG-salmon samples that was imaged each day with VMLite and on given days with VMLab, Except for the gill region which of only three gills from selected samples were imaged on given days. The red circles indicate the approximate skin-region that was imaged, gills where imaged by cutting away the gill-lid, The entire eye was imaged on both sides.

Only two gills were imaged at the same day and different gills were imaged every measurement day to limit the effect of increased oxidation from exposed gills. Each fish was tagged for sample identification and to mark the side of the fish facing down on the ice and up. QIM measurement was done with a panel of 5 semi-trained assessors every other working day, meaning the same days as VM Lab images was taken. The QIM scores was judged based on the assessment scales in Appendix 1a.

Data extraction

The images of VM Lab2 and Lite taken of the neck, abdomen, and tail skin-regions was processed with a nCDA threshold segmentation made by using the procedure described in 3.7 Multispectral data processing. where darker skin, melanized scales and areas contaminated by extrinsic factors such as external light or shadow was removed. The silvery scales and lighter skin closer to the ventral area of the salmon was kept since this constituted the main area of the images. The mean spectral values were then extracted from the segmented image. For region one and two (eyes and gills) a region of interest (ROI) was applied manually on each image. A circular ROI area was used to extract data from the pupils of the eyes and a line ROI was used for the gills.

VMLab2 and VMLite operates with a different set of wavelength-bands and light setup which means that separate segmentation files had to be made for each device. Considering the time needed to make segmentations and extract data it was decided that only the images of the skin regions from VMLab2 would be processed within the time-scope of this thesis.

3.6 Storage trail experiment two

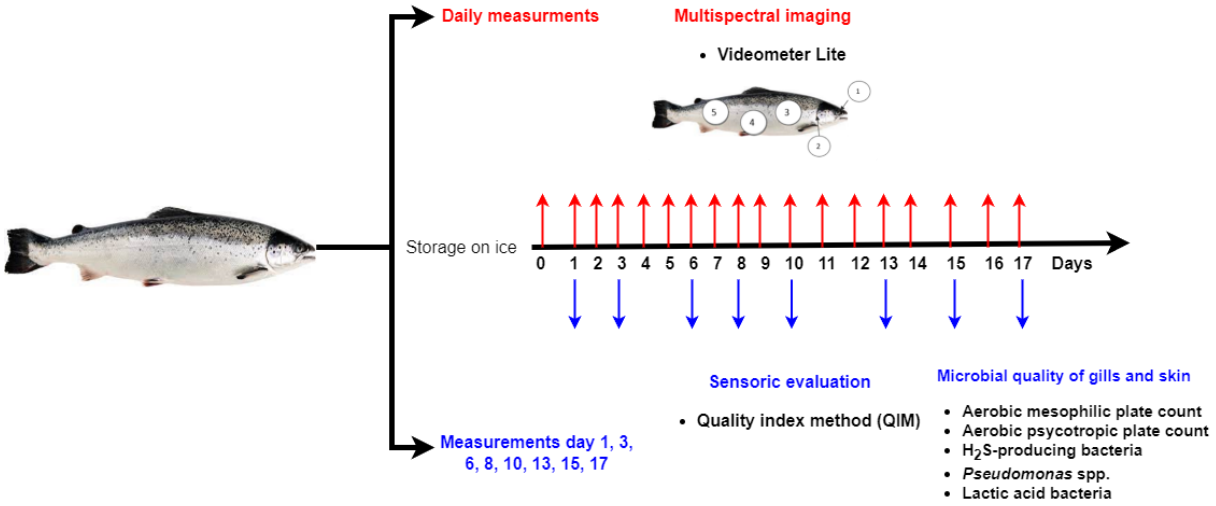

Figure 3-5 Shows the experimental setup for storage experiment two. Red markers show the measurement that was done daily which was imaging with VM Lite. Blue markers show measurements that was done on designated days which were day 1, 3, 6, 8, 10, 13, 15, 17. Microbial sampling and sensory evaluations with the QIM-method was done on these days.

A total of 20 whole HOG salmon of superior quality from Lerøy AS was used in the experiment. Measurements with VM Lite and QIM was done with accordance to the first storage experiment with one exception being that the same operator was responsible for imaging. This was done to reduce any variance of imaging techniques and give more consistent measurements.

To limit microbial cross-contamination of the samples and simulate ordinal storage on ice, the samples were separated in two groups. The first group stated with five HOG-salmon samples and was used for MSI and QIM -measurements. The second group started with 15 HOG-salmon samples and was used for microbial measurements. Microbial measurements were done every other day as described in Figure 3-5, and three HOG-salmon was sampled on each day. Sampling was done on the side which faced away from the ice and the fish was turned on the other side after sampling. This was done to allow the non-sampled side of the fish

(which had been facing the ice) to have the same temperature conditions as the other side before it was sampled on the next sampling day. When the microbial sampling had been done on both sides of a sample set, the three HOG-fishes was placed in the first group and measured with MSI and QIM. This means that the MSI and QIM sample pool was increased by three samples every other QIM and microbial sampling day.

MSI was done with the VM Lite prototype each day of the experiment's duration by the same operator for consistent imaging technique. Data processing was done in accordance with storage trail one, with the same segmentation files being applied.

3.6.1 Microbiological analysis

Microbial samples were taken of gills by cutting off a single gill arch with sterilized scissors and placing it in a petri dish for further processing. Skins were sampled by using a 34x16 cm sterile cloth dampened with peptone solution (SodiBox, Bretagne, France) to swab the entire side-profile of the HOG salmon. Sample material was then put in stomacher bags, diluted 1:10 with sterile peptone water, and homogenized using a Smasher© stomacher (AES Laboratorie, bioMériux Industry, USA) for 30 seconds. Homogenate was then transferred to sterile centrifuge tube and diluted in a series of five exponentially (10^{-n}) decreasing dilutions. The dilution factors were adjusted over time to accommodate increasing microbial growth on the samples. The dilution series were then plated on the four different agars listed in Table 3-2. The culture media were prepared in advance according to NMKL method No. 184 (Nordic-Baltic Committee on Food Analysis c/o National Veterinary Institute, 2006).

Table 3-2 Culture media used in the experiment, their target microorganisms and incubation conditions.

Culture media	Target bacteria	Incubation conditions
Long and Hammer agar (L&H)	Aerobic Psychotropic bacteria	15°C for five days
Iron agar	Aerobic mesophilic bacteria and H_2S producing bacteria	22°C for three days
De Man, Rogosa and Sharp agar (MRS)	Lactic acid producing bacteria (LAB)	25°C anaerobically for five days
Pseudomonas agar	*Pseudomonas spp.*	25°C for 2 days

The microbial concentration from gill samples is presented as log colony forming units per gram sample (Log CFU/g). Concentrations for the skin samples are presented as log CFU/skin as the exact area that was swabbed is not known.

3.7 Multispectral data processing

All images taken with the Videometer's multispectral imaging instruments were processed with the VideometerLab software for data extraction. The following content describes the process of how data was extracted from the raw multispectral images taken with the instruments.

Creating image segmentations for selective spatial information.

In order to extract information on an area of interest for a large number of sample images, the tool MSI Transformation and MSI Segmentation was used to detect

and segment out unwanted parts of the image. This process started with selecting a few representative images of the sample.

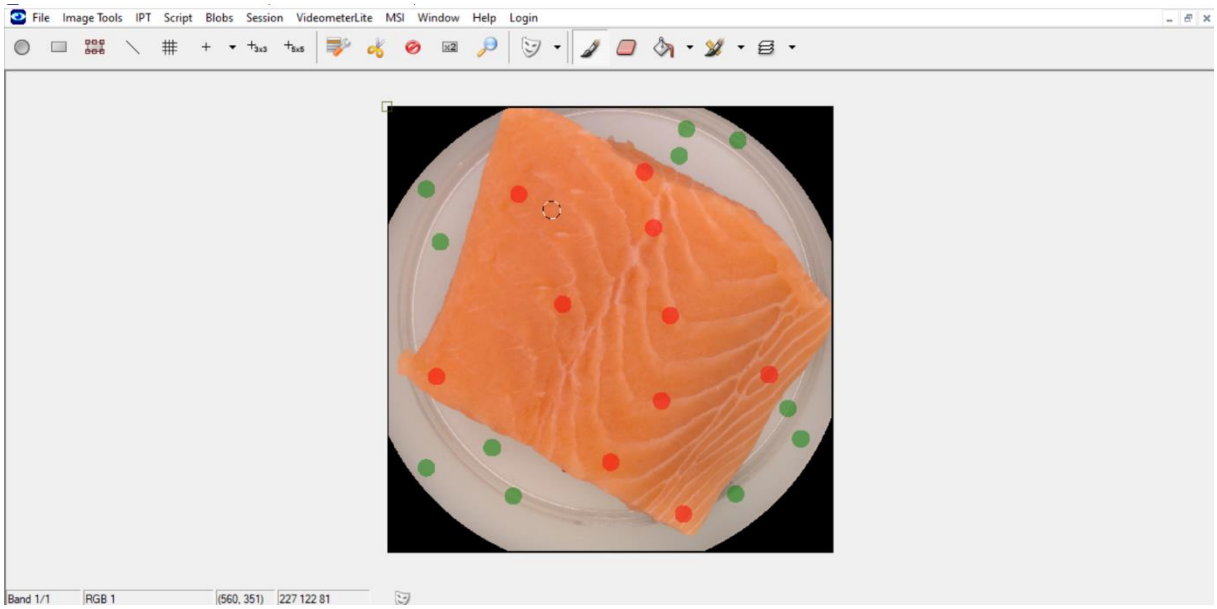

Figure 3-6 Shows an example of how images were marked for making the nCDA transformation. Red marks were used for the region of interest and green marks were used for marking background.

Then the pixels within the interesting parts of the sample was painted and classified as layer 1. The uninteresting parts of the sample was also painted and classified as layer 2 as shown in Figure . When enough representative images had been painted and classified the MSI Transformation builder was used with the nCDA method to calculate the wanted pixel classifier.

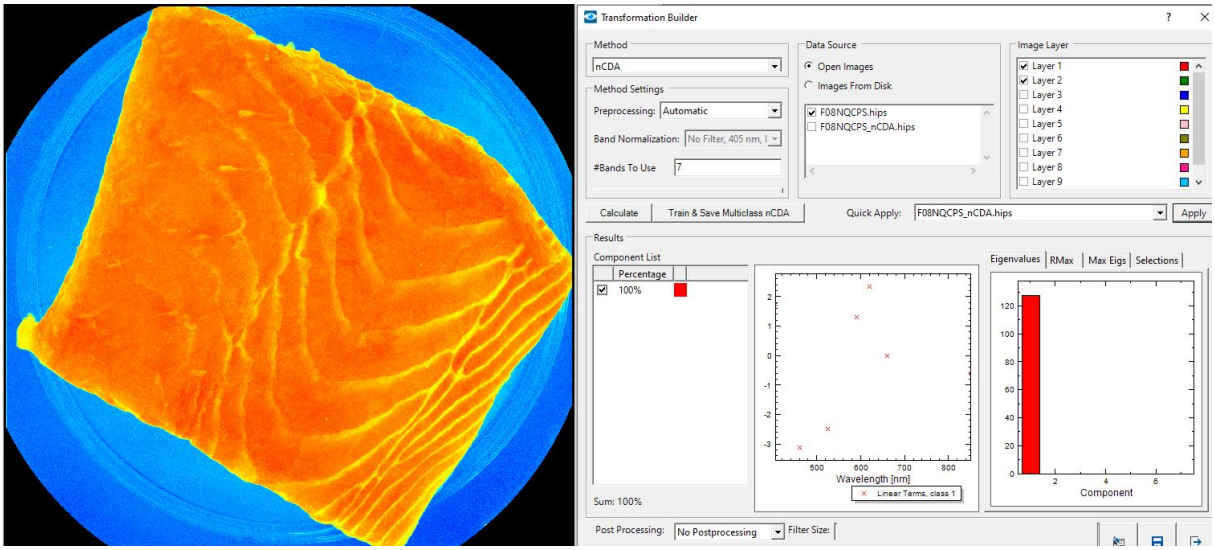

Figure 3-7 On the left side shows the resulting image of the nCDA pixel calculation with a colour gradient from red to blue marking the certainty of each pixel belonging to class 1 (red) or class 2 (blue). The right side shows the Transformation builder menu.

The transformation was applied and examined on the sample images to ensure correct classifications of the samples as shown in Figure 3-7, where a colour heat map of the nCDA pixel classification can be applied to the sample image. The colours represent the certainty of which of the two classes the pixel belongs. In the example of Figure 3-7 shows that the red pixels belong to the salmon fillet class of pixels and the blue pixels belongs to the background class. When the nCDA transformation satisfied the requirements for separation of different classes the file was saved and used for the next step.

In this next step the goal was to create a segmentation file based on the transformation that was made earlier. The segmentation builder 2 in VideometerLab software (Ver. 13193) was used for creating segmentation files.

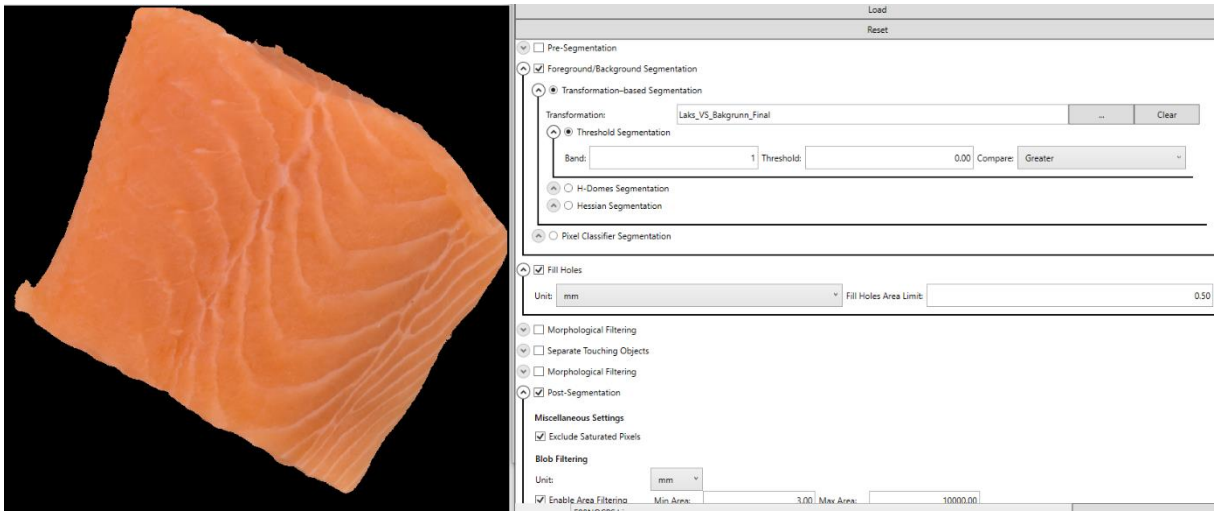

Figure 3-8 The result of a segmented image is showed on the left side. The menu of the segmentation builder 2 and parameters used is showed on the right side.

The foreground/background segmentation was selected with a transformation-based segmentation. Then the appropriate transformation-file was selected, and the threshold Segmentation method was used. The unit for threshold comparison was set on greater for all segmentation, but the value of threshold comparison was decided for each individual segmentation and based on sample testing. Other parameter that was used was under post-Segmentation, where in most cases the Area Filtering was used to remove small artifacts or concentrate the segmentation on large "blobs". For testing the effects of the segmentation it was applied to chosen sample images and evaluated. Figure 3-8 shows the effects of a background segmentation on a piece of salmon fillet, the segmentation removes the background and enables the whole fillet to be analysed. Adjustments of the

parameters was applied, when necessary, until the segmentation was able to select the entire region of interest.

Sample session for fast extraction of data

The tool "session manager" was used to extract spectral and colour data from a whole set of sample images with or without segmentation. In the cases where segmentations were used the effect of segmentations on each image was monitored during the session processing. Sample images where segmentations did not meet the requirements were noted and any necessary corrections was made.

3.8 Statistics

All multispectral image values extracted with Videometer Lab software is an average of all included pixels in the image. All values presented are mean values unless stated otherwise. Statistical analysis was performed with IBM SPSS Statistics, version 27 (IBM, New York, USA). One-way ANOVA was used to check for statistical differences and Tukey post hoc test was used to check differences between groups. Person's correlation coefficient was used to test for correlations between spectra and quality parameters. The statistical level of significance was set to 5% (α=0.05). Microsoft Excel was used for graphing.

Table 3-3 Pearsons Correlation coefficients and the corresponding relationship (Evans, 1996).

Scale of correlation coefficient	Value
0<r≤0.19	Very low Correlation
0.2≤r≤0.39	Low Correlation
0.4≤r≤0.59	Moderate Correlation
0.6≤r≤0.79	High Correlation
0.8≤r≤1.0	Very High Correlation

4 Results

4.1 Imaging protocol evaluation

Two different imaging protocols were used to test the Videometer Lite prototype's ability to capture images directly on whole fillet samples. The direct imaging protocol used the VMLite placed directly on the area of interest. The control imaging protocol used a 10x10 cm cut-out piece of the same area of interest placed in a petri dish.

The results of colour measurement with VM Lite of 20 salmon fillets was utilized for evaluation and comparison of the two imaging protocols. Values from spectral bands and colour values (LCh) was used for comparison as seen in Figure 4-1 and Figure 4-2 respectively.

On the comparison of spectral bands, there is a significant difference ($p<0.001$) at the 5% α-level between all spectral bands of the two imaging protocols. Where the average spectral reflection of the controlled protocol was significantly higher than that of the direct imaging protocol as is seen in Figure 4-1.

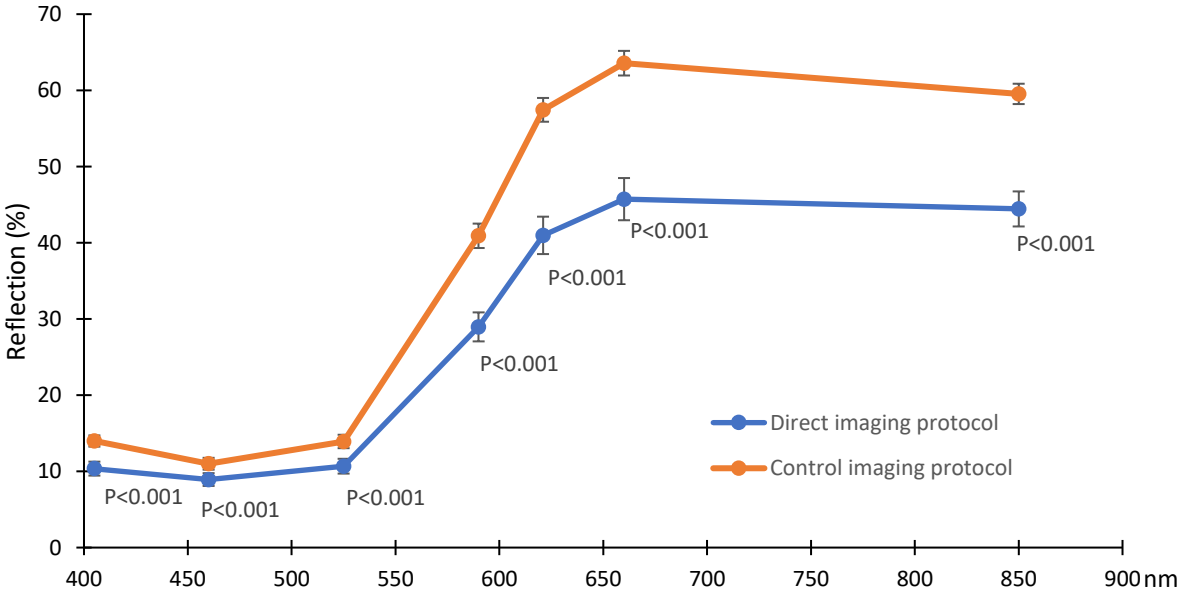

Figure 4-1 Comparison of the direct imaging protocol (blue line) and the control imaging protocol (orange line) mean spectra. Standard deviations are represented by error bars for each wavelength band. The ANOVA P-values are displayed for each spectral band and shows the significance of the mean difference in reflection between the two methods for each spectral band at α-level set to 5%.

The delta values between the direct and controlled imaging protocols were calculated to quantify the difference between the two protocols. It is seen that the difference in reflection between imaging protocols increases exponentially between 525 nm (3.2%) and 590 nm (12.0%) spectra, before flattening out from 621 nm (16.5%) to 850 nm (15,1%). Meaning that the red spectra (590-850 nm) had significantly higher reflection values for images taken with the control protocol compared to the direct imaging protocol.

For the colour values it was observed that both Lightness and Chroma had a statistically significant difference ($P<0.001$) between the two protocols, with the controlled method having a higher value in both cases of 59.1±1.0 L* and 57.3±1.7 C* against 48.3±1.7 L* and 49.3±1.65 C* for the direct protocol. No significant difference was observed for the hue-value at the $p<0.05$ level of significance. This meant that the control imaging protocol showed on average a brighter image (+10.8 L*) with higher colour saturation (+8 C*) and with similar hue (-0.9 h*) as the direct method.

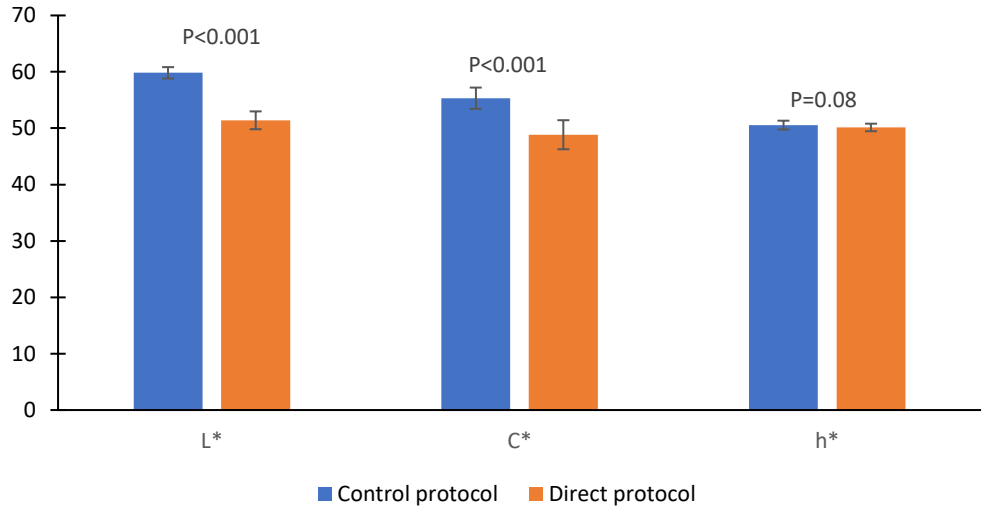

Figure 4-2 Shows the difference of the mean colour values Lightness (L*), Chroma (C*), and Hue (h*) between the control and direct imaging protocols. Standard deviations are represented by error bars. Significant differences from ANOVA can be seen for the L* and C* values at $\alpha=0.5$.

It was observed that the direct protocol had spatial sifts between spectral bands caused by movement during imaging. Dark and light areas around the integration sphere were observed in some images. Based on this fact an illustration was made to represent these factors shown in Figure 4-3.

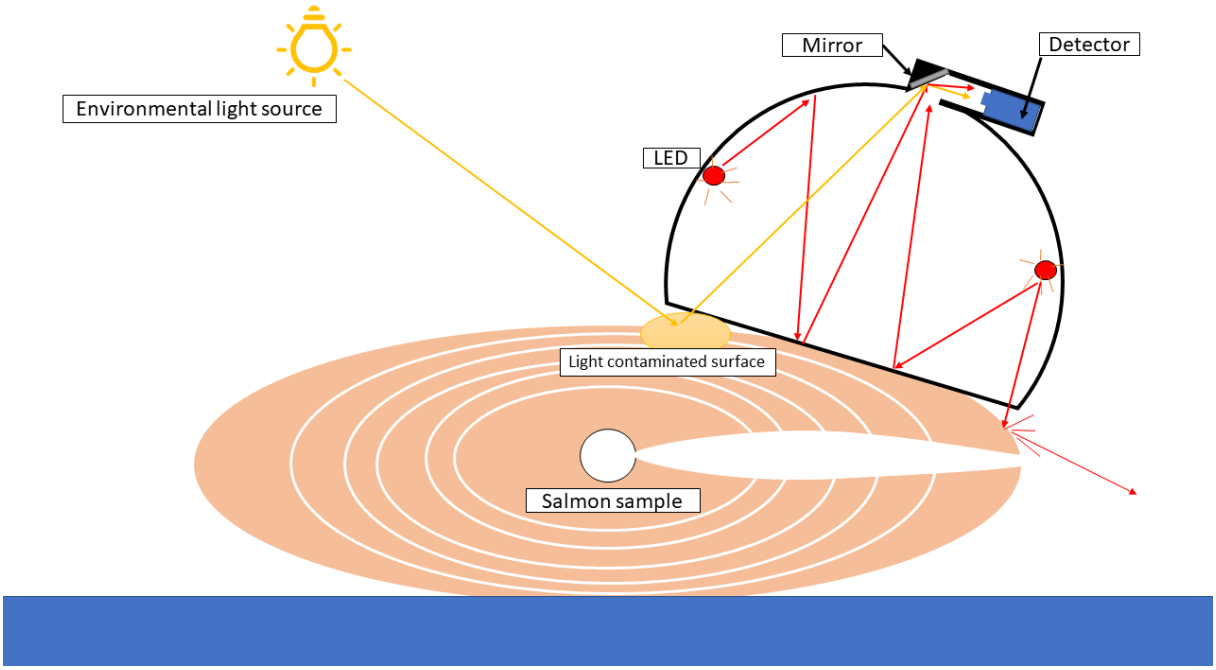

Figure 4-3 Illustrates the challenges of imaging a convex sample. This case demonstrates the imaging the belly area of a HOG-salmon in rigor. Visible gaps are seen on the sides of the bottom part of the instrument. On the left side of the instrument, environmental light is entering through the gap and reflected from the sample to the detector, causing light contaminated areas with high reflectance. On the right side, light from the LED's is not reflected into the detector creating shadowed areas with lower reflection.

4.2 Multispectral colour measurement assement.

The colour values of salmon fillets acquired from the VMLite prototype was tested against the measurements done with the DigiEye instrument. The results are displayed in Figure 4-4.

Overall, the VMLite shows significantly higher LCh values than that of the DigiEye instrument when control protocol was used. The average image of VMLite displaying a lighter colour (L*=59.1±1.0) that is more saturated (C*=57.3±1.6) and a hue angle turning more towards yellow (h*=50.9±1.0) than the redder hue that the DigiEye showed (h*=43.9±0.6). When the direct imaging protocol was used no significant difference was observed for chroma-values($p>0.05$). There was also a reduction in lightness (L*= 48.3±1.7) leading to a darker colour than the DigiEye value (L*=55.0±1.8).

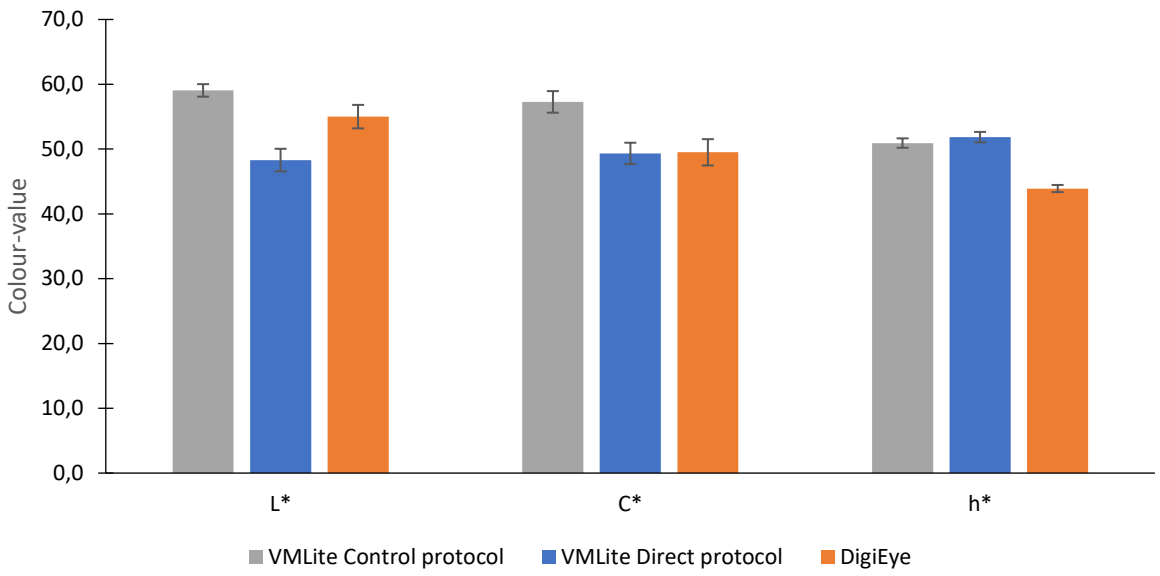

Figure 4-4 Shows the CIE LCh colour values for the Direct protocol and control protocol taken from salmon fillets with MSI VM Lite and DigiEye. Error bars represent standard deviations.

To investigate the difference in colour measuring of MSI and RGB with a standardized colour reference for each sample, the chroma values measured with the respective instruments of Roche SalmoFan™ was used to grade each sample with the SalmoFan scale ranging from 20-32 (pale pink to dark red, C* values are found in Appendix 2). The results of the grading with MSI and RGB data are posted in Figure 4-5.

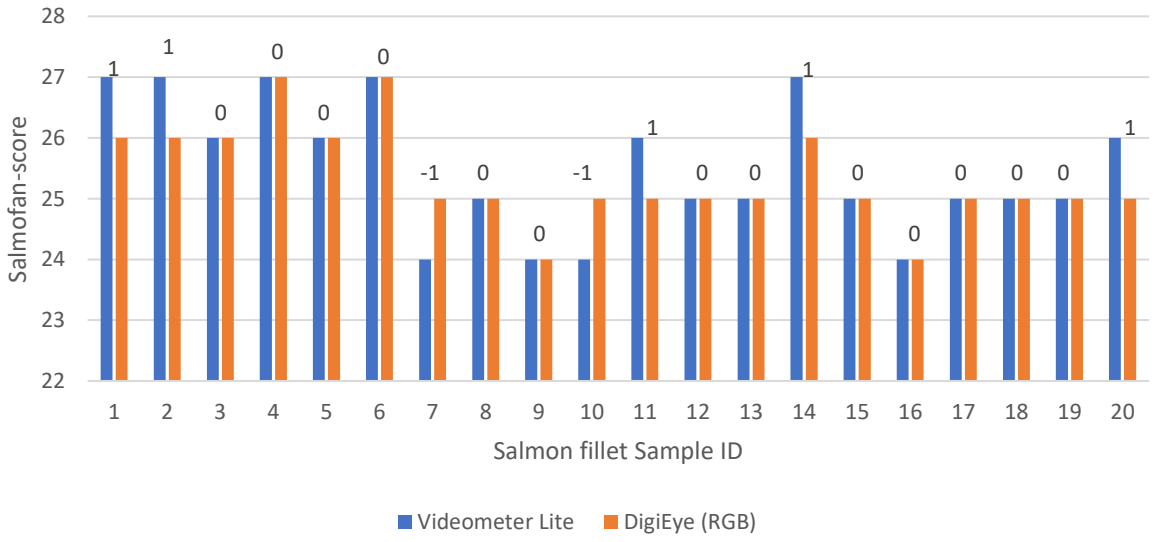

Figure 4-5 Shows the approximated SalmoFan™ score of VM Lite and DigiEye for all samples. SalmoFan™ scoring classification was based on approximating the measured chroma values of samples to the closest SalmoFan™ score cards chroma value. Annotated values represent delta difference in SalmoFan-score between VMLite and DigiEye

The results showed similar ranking of SalmoFan-score between the two instruments, with the average difference being 0.15 and the highest score difference of just one point. Seven of the samples had one score in difference between instruments while 13 remaining samples showed equal SalmoFan-score.

4.2.1 Astaxanthin content

Astaxanthin content was analysed of salmon fillet samples, results for astaxanthin concentrations of samples are listed in Appendix 3. Pearson's correlations coefficient was used to see if the data measured by the DigiEye and the VMLite instruments correlated to the measured astaxanthin concentration. The results from selected parameters are presented in Table 4-1.

Table 4-1 Presents the Pearson correlation between astaxanthin concentration and the parameters a* and C* taken by DigiEye and VM Lite, including the 460 nm and 525nm band from VMLite.

INSTRUMENT	a* (red-green)	Chroma	460 nm	525 nm
VM LITE	0.455	0.389	-0.272	-0.304
DIGIEYE	0.424	0.329		

Results show moderate correlations for the a-values (0.455) and low correlations for chroma (0.389), 460 nm (-0.272), and 525 nm (-0.304) of the VM Lite instrument. Other parameters such as lightness and hue are not shown since no correlation of any significance was observed. None of the values was statistically significant at the $P<0.05$ level, however the a-value of VM Lite came close with a p-value of $P=0.050$ (two-tailed). It was also observed that the VideometerLite instrument gave slightly better correlation than DigiEye.

4.3 Melanin detection

To figure out if and how the multispectral imaging device detects melanin spots in the salmon fillet, the average spectra of melanin spots were compered against the average spectra of the myotomes of the fillet as a reference tissue. The results are showed in Figure 4-6 for the spectral comparison of melanin and reference tissue.

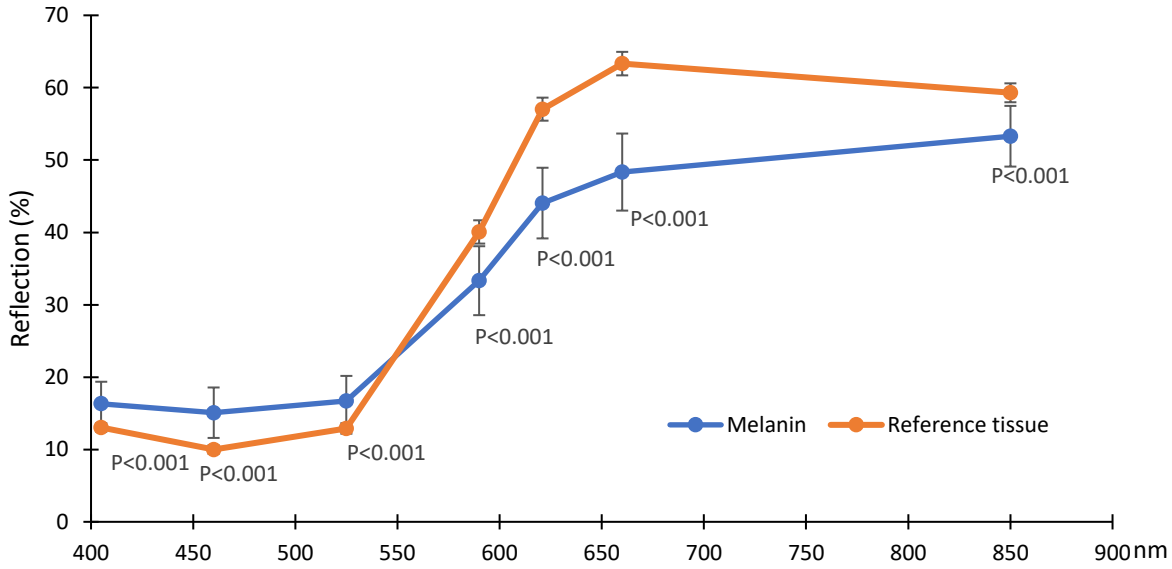

Figure 4-6 Comparison of the average spectra from 12 melanin spots (blue) with the reference tissue spectra of 20 salmon fillets (orange) using the control imaging protocol. Standard deviations for each wavelength band are represented by error bars. Annotated P-values was calculated by one-way ANOVA with a α-level of 5%.

The results showed significant difference between all spectral bands of melanin and the reference tissue for the controlled image protocol. It was also observed that melanized tissue had a higher reflectance at the UV-Cyan spectra (405 nm, 460 nm, 525 nm) and lower reflectance at the amber-NIR spectra (590 nm, 621 nm, 660 nm, 850 nm) than the reference tissue.

When comparing the spectra of melanin and reference -tissue with data from the direct imaging protocol, only the lower bands of 405 nm, 460 nm, and 525 nm plus 660 nm showed statistically significant difference at the 5% α-level from one-way ANOVA. The results are illustrated in Figure 4-7.

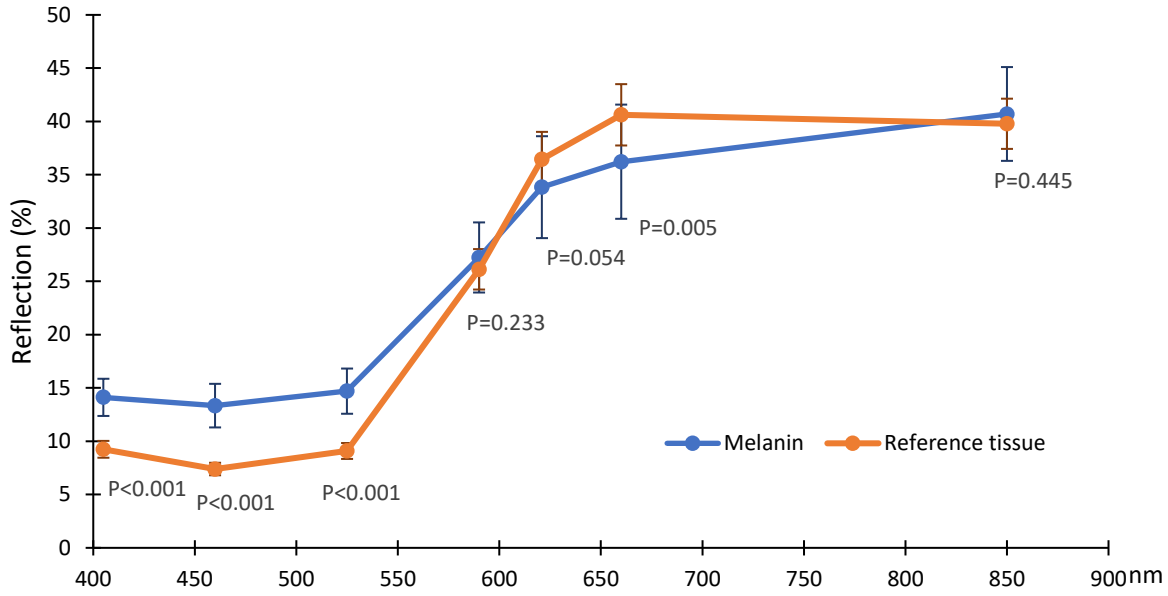

Figure 4-7 Comparison of the average spectra from 12 melanin spots (blue) with the reference tissue spectra of 20 salmon fillets (orange) using the direct imaging protocol. Standard deviations for each wavelength band are represented by error bars. Annotated P-values was calculated by one-way ANOVA with a α-level of 5%.

The LCh colour values extracted from the MSI images were also compared between melanin and reference tissue and is showed in Figure 4-8.

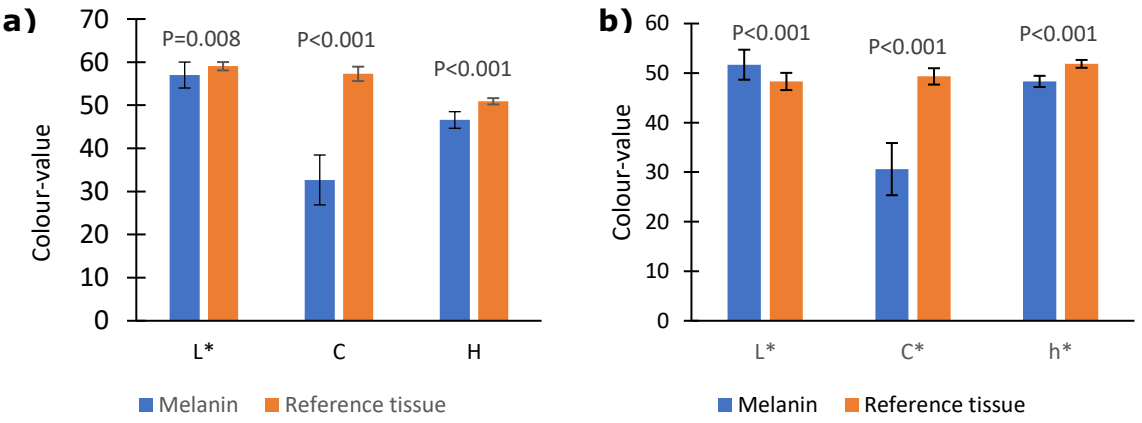

Figure 4-8 LCh values of melanin tissue (blue) and the reference tissue (orange) from the control imaging protocol (**a**) and the direct imaging protocol (**b**). ANOVA was used to calculate the difference of the two tissues for each colour value. The α-value was set to 5%.

The results showed that the melanin tissue has a significantly lower chroma value (32.7±5.7 C*) than that of the reference tissue (57.3±2.2 C*) ($p<0.001$), with a difference of 24.6 C* using control protocol values. There was also a significant difference for lightness and hue values, though the difference in lightness shifted between image protocols, melanin being slightly darker than the reference tissue in the controlled protocol and slightly brighter in the direct protocol.

4.4 Multispectral data of head-on-gutted salmon stored on ice

A total of five regions (Eyes, gills, neck, abdomen, and tail) of the HOG salmons were imaged over 21 days in two separate trails. The results of the spectral profile of gill, neck, abdomen, and tail regions from day 1, 8 and 17 of storage trail two are presented in Figure 4-10, the eye region is missing due to complications in data extraction.

The selected days represent the three classes of freshness based on the QIM-scheme score and are as such: Fresh (QIM-score<5), Matured (5<QIM-score<15), and spoiled (QIM-score>15). Corresponding average CFU/g are also presented for the selected days and are 3.6 log CFU/g, 6.7 log CFU/g, and 8.9 log CFU/g for days 1, 8, and 17, respectively. P-values for the difference between each wavelength band was calculated using one-way ANOVA with an α-level of 5%.

Spectra from the gills (Figure 4-10 a) showed a significant difference (p=0.005) at the 850 nm (NIR) wavelength. We can also see a change in the spectral reflection pattern between the days, where the overall reflectance drops from day one measurements to day eight before increasing above day one on day 17. The spectral changes coincide with the observed change in colour of the gills, becoming darker in appearance when matured before turning lighter and greyer when spoiled as seen in Figure 4-9.

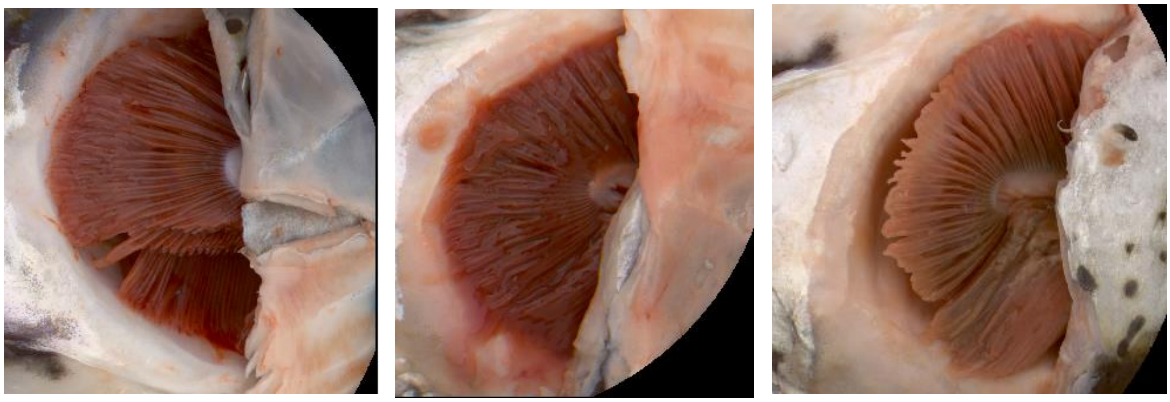

Figure 4-9 Images taken of gills on day 1 (left), day 8 (middle), and day 17 (right) With VMLite.

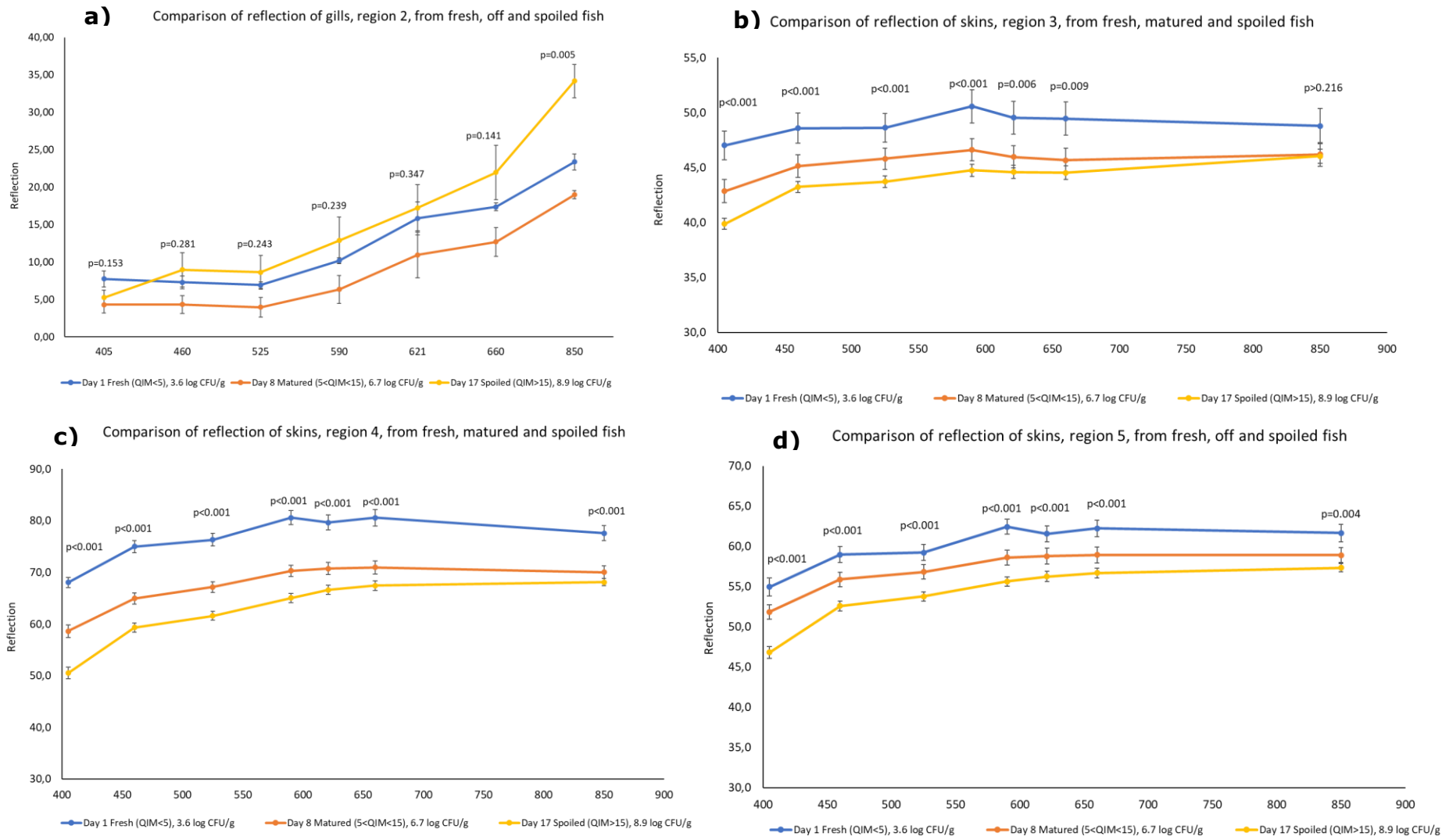

Figure 4-10 graphs that show the spectra taken with VMLite of the gill (**a**), neck (**b**), abdomen (**c**), and tail region (**d**) from storage trail two on day 1, 8, and 17. Error bars represent standard error. P-values are calculated from ANOVA with α-level=0.05 and shows the statistical difference between different days on each wavelength band.

The skin regions (neck, abdomen, and tail) spectra showed a clear trend of reduced reflection over time, as seen in Figure 4-10 b-d. The wavelength band that showed the best distinction for loss of freshness was 405 nm band, while the least difference was observed at 850 nm (NIR). All skin regions showed a clear significant difference between day 1 fresh, and day 8 matured and 17 spoiled. However, differences were smaller between matured and spoiled, especially at higher wavelengths as is well demonstrated in the tail region.

As seen in Figure 4-11 the shine and number of scales are clearly reduced over time, going from a bright shine to a darker more metallic/silvery shine and eventually becoming matt grey and having a severe loss of scales.

Figure 4-11 Show the degradation of fish skin. Images are taken of the tail region on day one (left), day 8 (middle), and day 17 (right). A clear reduction in the number of scales and shine of the skin can be seen from day 1 through day 17. Images presented are form sample ID 1 and in sRGB-format taken with VM Lite.

The abdomen region had the best reflection separation between fresh, matured, and spoiled, with significant differences ($p<0.05$) between all groups from 405 nm to the 590 nm band. The last bands from 621 nm to 850 nm only showed a significant difference between fresh and the other two classes but no difference between matured and spoiled. Overall reflections were also higher for the belly region then the other skin regions, which can be explained by the fact that only the silvery light-coloured scales and skin were measured, and the belly region is much lighter in colour and almost white compared to the other skin regions as seen in Figure 4-12.

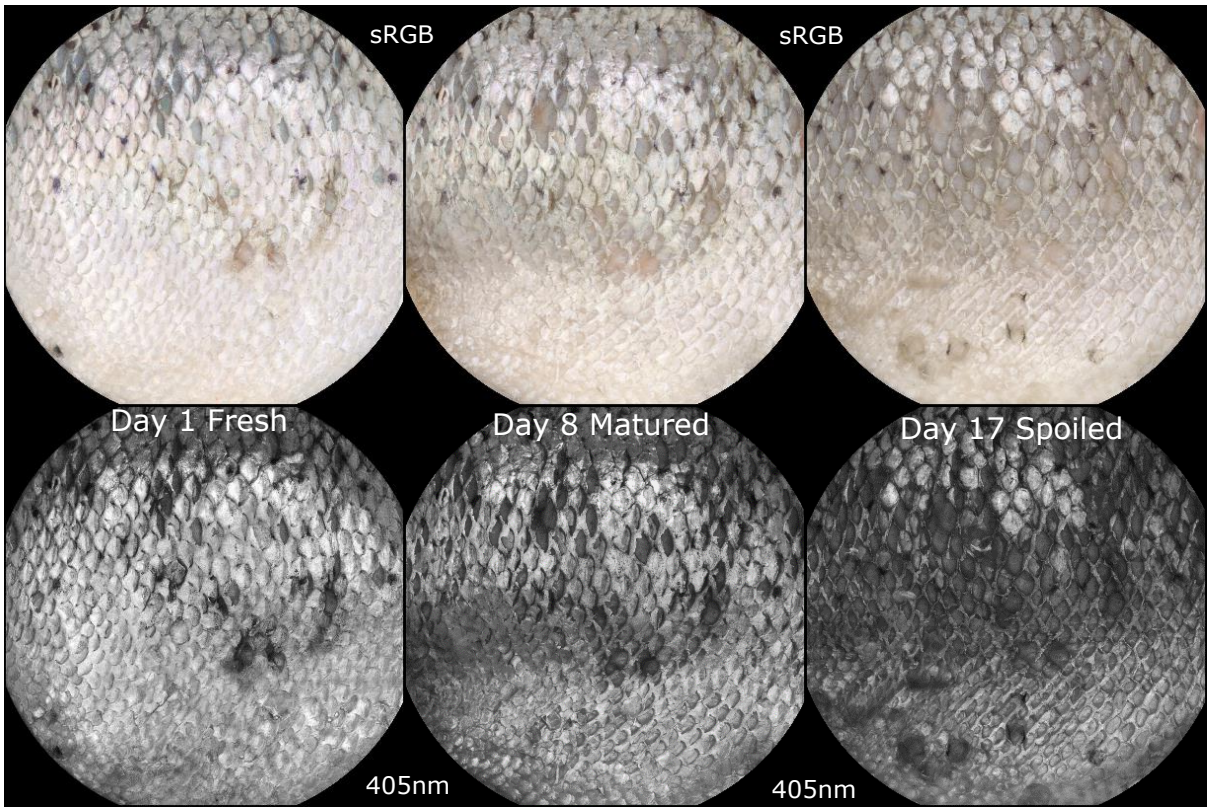

Figure 4-12 Images taken from VM Lite in storage trail two of the abdomen region from fresh, matured, and spoiled samples in sRGB-format and grayscale 405 nm reflection image. Notice the reduction of reflection in the lower half of the images over time in both formats.

4.5 VideometerLite prototype versus VideometerLab2

The spectra of the skin regions taken with VMLab2 and VMLite in storage trail one is compared to assess differences between the devices. The results will help with verifying the handheld prototype's performance against a more established instrument like the VMLab2. It can also help identify spectral signatures of salmon skin that is not covered by the VMLite instruments limited spectral resolution.

Results showing the spectra of the neck, abdomen, and tail skin regions taken on day 2, 9, and 18 of storage trail one with both MSI instruments are displayed in Figure 4-13 (A-C). The days that are represented in the results were chosen to detect differences between fresh (Day 2), matured (Day 9), and spoiled (Day 18). The degrees of freshness were assessed by the QIM-method.

The differences in reflection between VMLite and VMLab2 are clearly shown in the neck (A) and tail region (C), while the abdomen region (B) showed similar reflection values between the instruments. It was observed that the VMLab2 spectral profile is comparable between the regions having defined absorption

peaks at 570 nm and between 890 nm and 940 nm. Videometer Lite did show the same absorption peaks and had a relatively linear trend between the wavelength bands, though the two devices had similar trends in the abdominal region where both devices showed increasing reflections from 405 nm to 590 nm. The differences in overall reflection between the MSI devices seen in the neck and tail regions could be explained by different light-setups, meaning the strobe time and intensity of each LED. The VM Lab2 was equipped with diffused high-powered LEDs while the VMLite used diffused low-powered LEDs. In practise this means that the time it takes to acquire one wavelength band in a MSI is around ten times longer for the VMLite compered to VMLab2, which is done to correct for the lower LED light intensity of the VMLite. The strobe timing for the VMLab2 was adjusted using the tool Auto-light-setup to avoid light saturated pixels from the highly reflective scales of the salmon skin. The same tool was not available for the VideometerLite, though there seemed to be no issues with saturated pixels in the images. This explanation for differences in reflection was disputed by the results in the abdomen region, where reflection values of both instruments were at the same level.

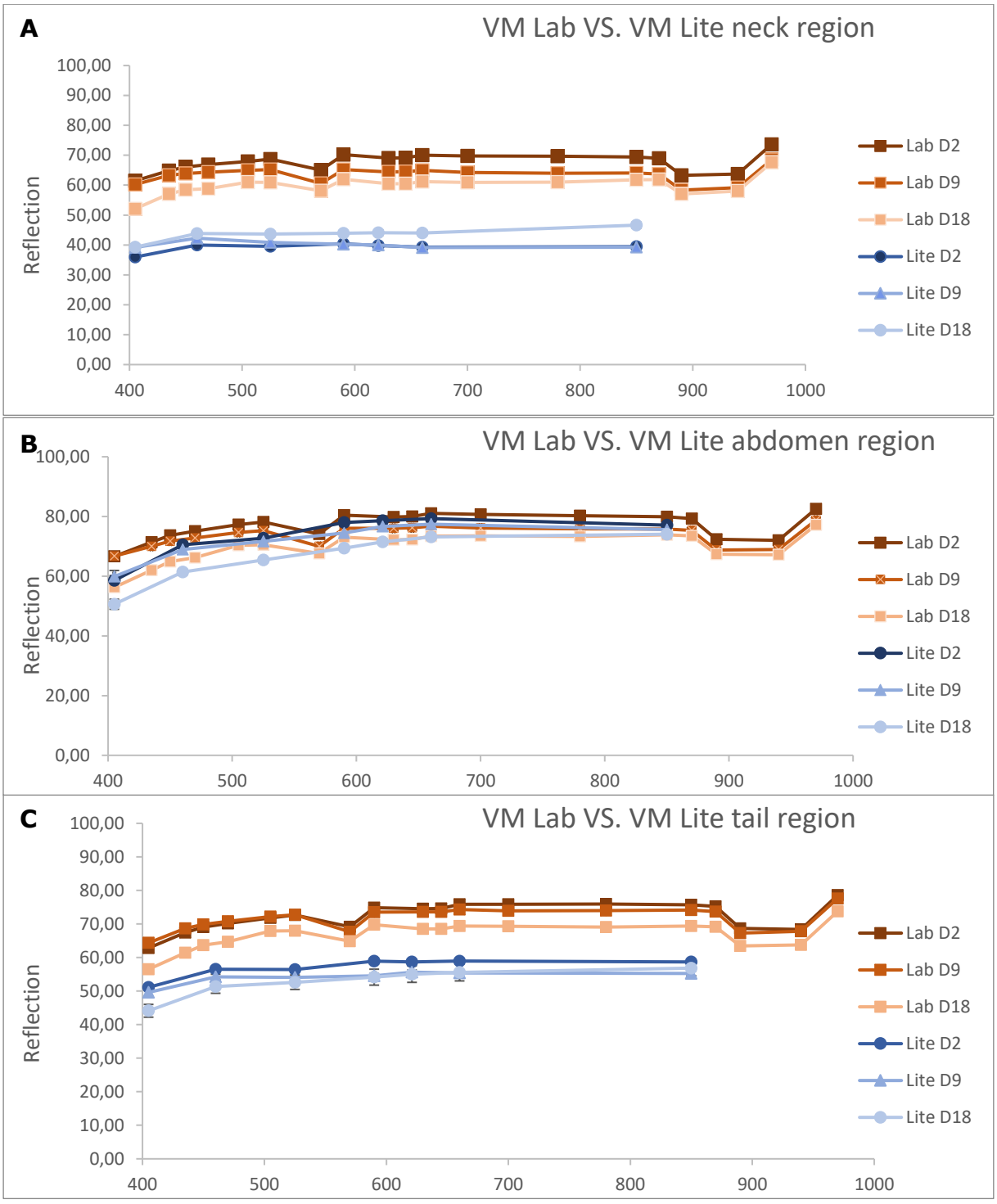

Figure 4-13 Shows the spectra of the salmon skin regions neck (A), abdomen (B), and tail (C) taken with VMLab2 (Orange Lines) and VMLite (Blue lines) on Day (D) 2, 9 and 18 of storage experiment one.

Another explanation may be different exposure to light from the outside environment because of differing methods of placing the instrument on the sample. As seen for comparing the direct and control imaging protocols, the direct imaging protocol led to reduced reflection values of the VMLite images. Due to the sensitivity of the VMLab2 to external light and the nature of the device, efforts

were taken to eliminate or severely reduce the influence of external light sources on the VMLab2 images. Another factor that explains the similarity in region 4 is that this belly region is more flexible and softer than the tail and abdomen, making a better seal against the VMLite image dome. Considering this, the most plausible reason for the differences of reflection between instruments in the neck and tail regions are more light contamination or shadows of the VMLite images.

4.6 QIM results and correlations with multispectral data

Eight QIM measurements was done over the timespan in both storage experiments. The total average QIM-score of HOG salmon samples stored on ice of both storage experiments is shown in Figure 4-14. As seen in the figure, storage trail one had, on average higher scores than the second storage trail. Some of the reasons are most likely due to the extensive fish handling during the experiments. In storage trail one all the HOG salmon was imaged every day with VMLite and every other day with both VMLab2 and VMLite.

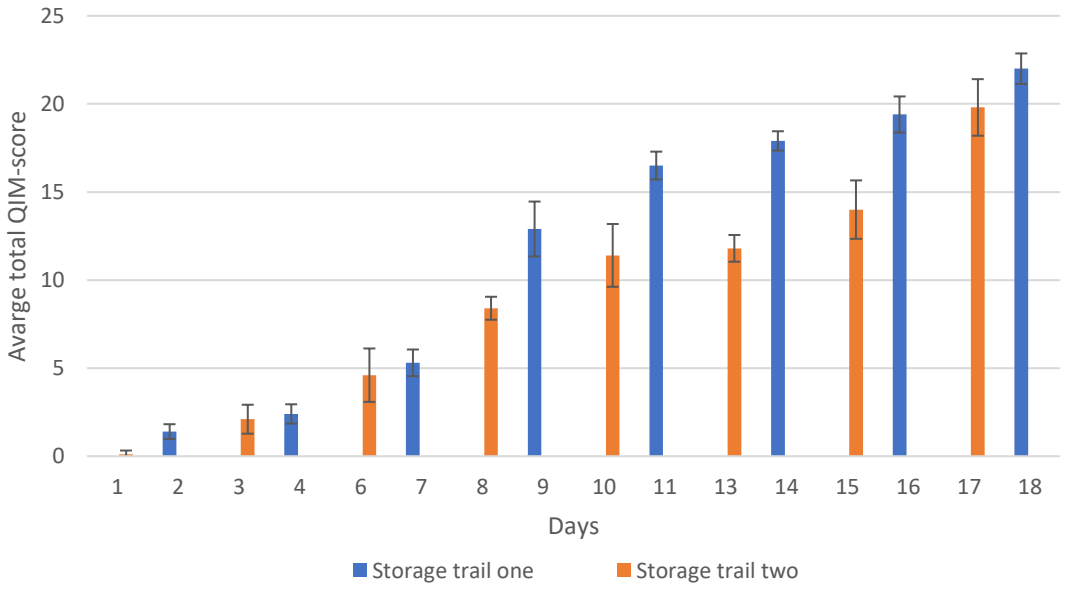

Figure 4-14 Shows the average total QIM-score measured throughout storage trail one and two. Values at 15 or above are considered spoiled according to appendix 2.

According to the QIM-methodology the HOG-salmon is spoiled and not fit for consumption when the total score reaches above 15 (Appendix 2). The average total score in storage trail one reached above 15 on day 11, while the average score in storage trail two reached above 15 on day 17.

QIM-score was correlated to spectral-values of the skin regions with persons correlation coefficient and is shown in Table 4-2. The results shows that there is a moderate to high negative correlation for abdomen and tail regions in both storage trails. The neck region had the lowest correlations on all wavelengths with only one significant low correlation (r=0.368) at the 5% α-level for the 405 nm band in storage trail two. The highest correlation was observed at the 405 nm band of the abdomen region in storage trail two (r=-0.792). It was also observed that correlation values tended to rise with decreasing wavelength bands, suggesting that the lower wavelength bands would be more suitable for predicting QIM-scores.

Table 4-2 Show the correlation between Total average QIM-score and skin samples spectra using persons correlation coefficient. * Marks the significance level of $p<0.05$, ** marks the significance level of $p<0.01$.

Analysis area	Replicate	QIM vs 405nm	QIM vs 460nm	QIM vs 525nm	QIM vs 590nm	QIM vs 621nm	QIM vs 660nm	QIM vs 850nm
Neck (3)	1	0.002	0.082	0.147	0.134	0.142	0.148	0.276
Abdomen (4)	1	-0.429**	-0.576**	-0.495**	-0.511**	-0.546**	-0.477**	-0.367*
Tail (5)	1	-0.609**	-0.639**	-0.520**	-0.520**	-0.504**	-0.492**	-0.412**
Gills (2)	2	-0.547**	0.254	0.361	0.408	0.137	0.394	0.696**
Neck (3)	2	0.368*	0.147	0.133	0.121	0.072	-0.060	0.002
Abdomen (4)	2	-0.792**	-0.714**	-0.714**	-0.665**	-0.564**	-0.526**	-0.481**
Tail (5)	2	-0.596**	-0.519**	-0.484**	-0.510**	-0.435**	-0.439**	-0.385*

4.7 Microbiological analysis

Results of microbial analyses are shown as microbial growth curves in Figure 4-15 for skin samples and in Figure 4-16 for gills. The highest microbial counts were found for psychotropic aerobic microorganisms in both gills (8.9±0.2 log cfu/g) and skin (>9.2 log cfu/skin) samples on day 17. This included all organisms that are psychrotolerant and heat labile, which also includes *Photobacterium phosphoreum* (NMKL, 2006). It was also observed that H_2S-producing bacteria, *Pseudomonas spp*. and general aerobic bacteria had similar growth patterns. Lactic acid bacteria were sparsely detected on the MRS agar.

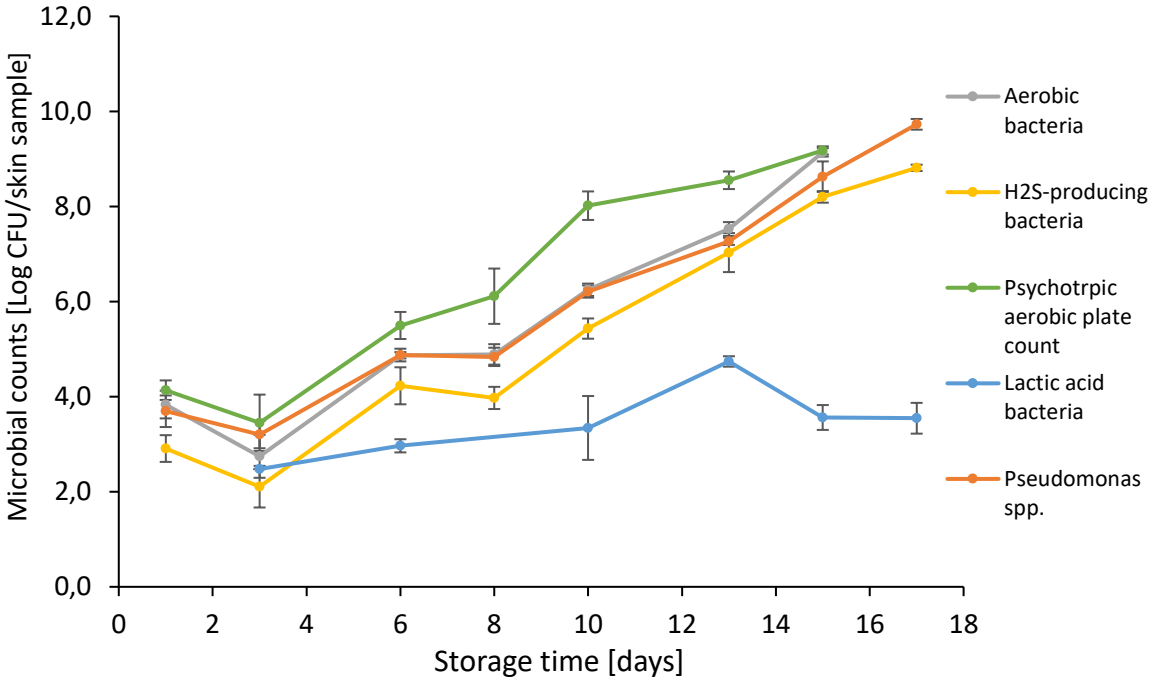

Figure 4-15 Average microbial counts of skin samples for psychotropic aerobic (green), H_2S-producing (yellow), aerobic (grey), Pseudomonas spp. (orange), and lactic acid bacteria (blue). The values are given as log CFU/skin and storage time in days. Standard deviations are represented with error bars.

A high correlation between microbial growth on salmon skin and the 405 nm band were found (r>0.6, Appendix 4) with some exceptions.

For *Pseudomonas spp*. the highest correlation (r=-0.774) was given at 405 nm of the tail region, while the abdomen region had a close correlation value at the same band of r=-0.738. The neck region had low non-significant correlations on all bands for *Pseudomonas spp*. All other wavelength bands of the skin regions had low to moderate correlations with the growth of *Pseudomonas spp*. and at no statistical significance (p>0.05).

The total aerobic counts show similar results as *Pseudomonas spp*. though the abdomen region had the highest correlation in this case at r=0.625, being the only statistically significant correlation of the skin regions at 5% α-level.

For H_2S-producing bacteria the highest significant correlation was achieved at 405 nm of the tail region with r=-0.719 (p=0.008). The only other significant correlation was of the abdomen region at the same band, with an r-value of -0.634 (p=0.027).

For psychrotrophic aerobic bacteria there was only one significant correlation which was at 405 nm band of the abdomen region, with an r-value of 0.614 (p=0.034).

The microbial sample replicates of gills had higher variances compared to the skin samples, as can be observed in the high standard deviations of Figure 4-16. Also, H_2S- producing bacteria had a less consistent growth pattern for gills than on skin. This indicates that there is more variation between samples for the gill microbiota compared to skin samples.

Microbial counts of salmon skin correlated well with the average QIM-score, giving a very high corelation value ($r>0.9$, $p<0.001$) with all microbial counts except lactic acid bacteria (Appendix 4).

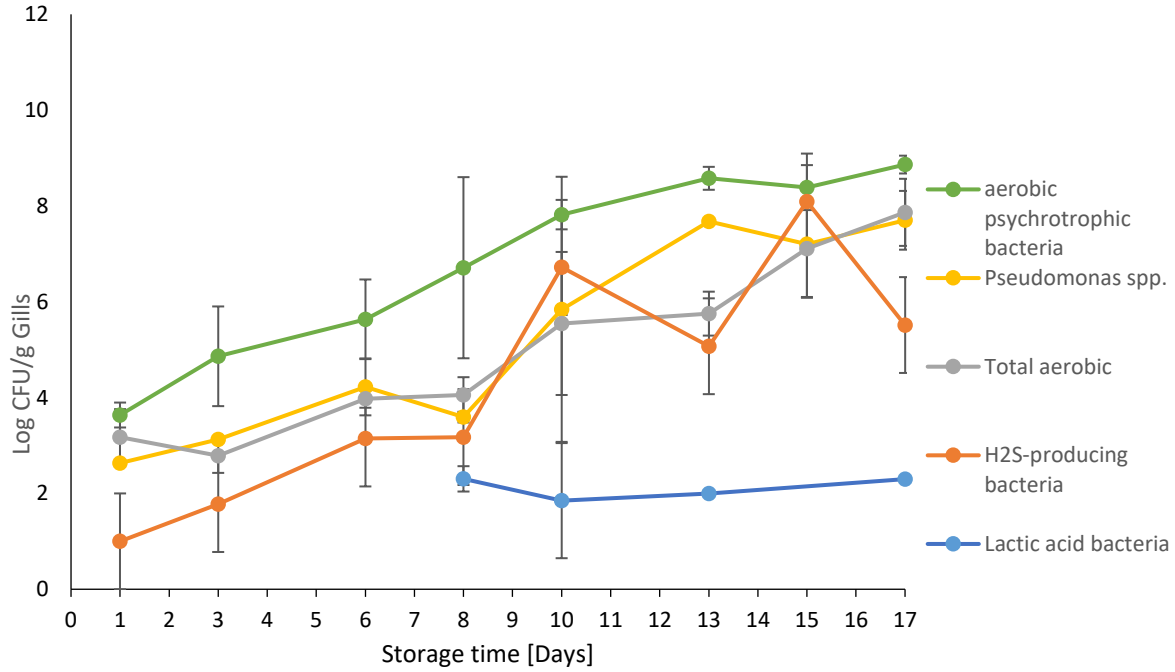

Figure 4-16 Show the average microbial counts of gills for psychotropic aerobic (green), H_2S-producing, aerobic, Pseudomonas spp., and lactic acid bacteria. The values are given as log CFU/g and storage time in days.

Correlation of gill spectra with microbial counts showed differing correlation than that of the skins. The most interesting results were that there was significant high correlation at the 850 nm wavelength band which is on the opposite side of the spectrum that skin samples correlated. Although significant correlations of gills and microbial counts were found on the 405 nm band in all cases as well.

The highest correlation between spectral bands and microbial counts of gills were for total aerobic counts at 850 nm with an r-value of 0.750 ($p<0.001$), there were also a high correlation for *Pseudomonas spp*. at the same spectral band at $r=0.732$ ($p<0.001$). Correlations at 405 nm bands for gills had r-values that ranged from --0.455 (total aerobic) to -0.627 (total psychotropic aerobic).

It was noted that only the non-visible spectra of UV and NIR gave high correlation to microbial growth and that UV-spectra had negative correlation with sinking spectral reflection and rising microbial counts, and NIR-spectra had positive corelation where both factors increased.

5 Discussion

5.1 Validation of multispectral imaging protocols and colour messurements

The aim of the TraceMyFish project is to find ways to utilize the VideometerLite prototype for quality measurements of fish. For this purpose, it is relevant to find a protocol for using the device. An important selling point of the VMLite is its mobility and making it able to take multispectral images in the field, and the non-destructive nature of spectral imaging. These factors will be considered when evaluating the protocols.

As it was showed in the results of chapter 4.1, the controlled protocol gave in general significantly higher reflection than that of the direct protocol. Some of the factors that are suspected to affect the results of the direct on-sample protocol are: the movement of the instrument during image capture due to unstable surface and/or handling by the operator, and contamination of images from external light sources and/or shadows caused by gaps or indentations between sample and instrument.

The movement of the instrument during imaging with the direct protocol are showed clearly in all images, by viewing and comparing the grayscale converted image from every band of a single image in chronological order (405nm-850nm), any movement between the bands should be observed. The severity of the movement in each case is hard to define as this would require a qualitative investigation of each image which is out of the scope for this thesis. However, this issue may be resolved in future updates of the VM software that can correct the movement between the bands as suggested by Videometer official Carstensen (2022).

The cause of the movement is believed to come from multiple factors. These being the loose and flexible surface of the fillet, on which the device is supported by during imaging, and the movement caused by the operator pushing the image capture button at the top of the device. The fact that the operator needs to hold

the imaging device to stabilize it during image capture is also considered to be an important factor for movement. In all cases it is safe to assume that operator and device interaction during imaging is the main cause of movement and misaligned spectral bands. Alternative solutions that could in some cases be implemented to fix the issue are to limit interference from the operator with the spectral imaging device during capture, but this is only possible if the instrument is able to hold itself stable without any large gaps between the sample surface and device.

A gap between the bottom part of the imaging device and the sample surface may let light from the outside environment to reflect of the sample surface and onto the device's camera. This is illustrated in Figure 4-3 which demonstrates how outside environmental light and gaps can affect the sample surface.

The results showed quite clearly that the effect of the direct protocol reduces overall reflection of all bands though the difference did increase with higher reflection values. The average spectral profile between the two protocols showed similar patterns with low reflections at the lower wavelengths and high reflections the higher, redder wavelengths. However, when the difference between melanin tissue and muscle tissue was compered the image protocols showed a significant impact on the results, where the control protocol had a clear difference between each band, the direct protocol showed fewer significant spectral differences between the two tissues. This suggest that the previously mentioned image disturbance factors of the direct method can change the spectral profile of samples enough to make tissue separation and identification more difficult and less accurate.

One crucial factor that must be considered between the protocols are the background used during imaging with the controlled protocol, or the lack of background in the case of the direct protocol. The results of the salmon spectra make it clear that reflectance changes more between protocols within the salmons' visible spectra i.e., the red spectrum than the bluer spectrum. This means that the difference between protocols comes primarily of differing light intensity since more light is reflected and absorbed by the sample in the control protocol compared to the direct. The most likely factor for this increased light intensity is that the white background of the controlled protocol helped reflect more light from the LEDs on the sample which increased the reflectance. The direct protocol did not have any surrounding background since the entire image opening of the VM Lite was covered

by the sample. This then led to overall higher absorbance for the direct protocol, especially in the red spectrum because of the colour of the sample.

Considering this it could not be determined if the direct image protocol is accurate or not as the control protocol may be influenced by the sample backgrounds reflective properties. The previously mentioned factors of light/shadow contamination and image movement effect on the data results for the direct protocol could also not be determined. The best supporting evidence for that differing light intensity due to reflective background is the main factor of difference between protocols can be viewed in chapter 4.5, where VM Lab2 was tested against VM Lite. The results of this test suggested that the overall decreased reflection of the VM Lite sample spectra compared to the VM Lab2 was because of the VM Lite relatively lower powered LEDs. These facts coincide with the results of the image protocols, and it would be fair to suggest that the higher-powered LEDs of VM Lab2 may give better results when using the direct image protocol as was seen in the results of chapter 4.5.

The VM Lite performance in colour measurement of salmon fillets was tested and compared with traditional RGB colour imaging and the results of these test are described in Chapter 4.2. Salmon fillet colour is an important quality criterion and has an impact on the commercial value (Alfnes et al., 2006; Anderson, 2000; Koteng, 1992; Zheng et al., 2021). Therefore, the ability to accurately determine and grade the colour of salmon fillets in line with human colour perception would be beneficial to stakeholders within the value-chain. The current sensory method of using a colour card reference is fast, but also labour intensive and prone to bias. It would be more effective to employ a digital measuring system that is able to measure colour and colour changes of each individual fish throughout the value chain. There are several systems capable of colour measurement like RGB cameras and MSI. Since MSI have several advantages over traditional RGB imaging like the possibility to measure other quality factors such as texture, fat content, and more (Downey, 1996; ElMasry et al., 2011; Nilsen et al., 2002), it would also be beneficial to also measure colour of fillets with the same system.

To validate the VM Lite instrument for colour measurements of salmon fillets, it was tested against a RGB camera-based colour measurement system that uses a light box which simulates the CIE standard D65 illumination of the sample. While the MSI instrument uses the measured spectral bands and converts it digitally to

standardised CIE Lab and LCh images with simulated D65 illumination. This means that the colour converted images of the MSI device digitally simulates the daylight conditions for colour representation, while the RGB colour measurements system creates the same daylight conditions using calibrated lamps. This gave a comparison between physically simulated lighting conditions with broadband RGB imaging, and digitally converted colour images with simulated lighting conditions based on seven different wavelengths. The values of the LCh colour standard were comparatively to RGB imaging significantly higher on all points for the MSI instrument. This means there is a different representation of colour between the two instruments when following the CIE standard. The difference in colour may be a result of the different methods of applying the D65 illuminant. As stated by CIE (2004) there is no recommended artificial light sources to realize the D65 illuminant. However, later research by Hirschler et al. (2011) concluded that filtered tungsten lamps like the ones in the RGB colour measurement system used in this thesis provide excellent D65 simulators in the visible spectral range. This is also stated in a later review by Hirschler (2016). The MSI unit applies the CIE D65 illuminant on the calculation of tristimulus values from the spectral reflectance measured as described in section seven of CIE (2004). It can be argued that the MSI imaging systems lack of need for an artificial D65 light source is advantageous since it is not prone to any deficiencies or maintenance that is associated with fluorescent lighting. Also, LEDs are reported to be much more reliable and have higher accuracy compared to halogen lamps (Blanch-Pérez del Notario et al., 2020; Herrera-Ramírez et al., 2014). It is difficult to assess whether RGB or MSI are better for colour assessment of salmon as there is limited research on this topic. However, the results where the chromaticity of salmon samples taken from RGB and MSI instruments was ranked after the chromaticity of the Roche SalmoFan™ showed that there is a low difference between the two instruments when using a common reference. Though this comparison only used the C* value to rank the samples after the SalmoFan™-score a more accurate approach may be to use a another colour index like the Meat Redness Index (RI=a*/b*), which can be used to monitor the change in redness between samples (CHEN et al., 1997; Pathare et al., 2013). The reason chroma was used for SalmoFan-score ranking was due to the different gradients of the fan showed a clear positive trend between chroma and score. Lightness also showed the same type of trend but in smaller intervals

compared to chroma. Hue-angle was similar across the SalmoFan-gradient and as such was not suited to be used for classification.

Another interesting quality parameter regarding colour is the measurement of astaxanthin pigment content in salmon fillets. The salmon farming industry has long struggled with achieving high colour saturation in fillets and the amount of astaxanthin in the feed of salmon has doubled since 2005 (Aas et al., 2022). Astaxanthin supplements in feed are costly and makes up for around 15-25% of the total feed cost (Amoroso et al., 2020). The ability to easily measure and get real-time values of Ax-content in the salmon value chain is very lucrative, since stakeholders could potentially get a better understanding of the correlation between the effects of feed, environment, and handling has for the deposition of Ax-content in fillets. For this reason, the astaxanthin content from salmon fillets of the colour experiment was analysed by using HPLC. The results of the Ax analysis were correlated with tristimulus values and spectral data from the same fillets using persons correlation coefficient. This experiment resulted in moderate correlations with no statistical significance, it was observed that the a*-value had the highest correlation value (r=0.453) while the highest correlation values from the spectral bands was from 460 nm (r=-0.271) and 525 nm (r=-0.302) which was expected due to pure Ax having peak absorption between 450 nm and 600 nm (Buchwald & Jencks, 1968). The low correlation values may be caused by the high uncertainty of the chemical determination of Ax in salmon fillets, since only 3 grams of sample material was used from each sample. Results could have been more accurate if a larger quantity of sample material had been analysed and duplicated or triplicated which is more in accordance with source material (Dissing et al., 2011; Vecchi et al., 1987). The ability to measure Ax in rainbow trout by multispectral imaging was researched by Dissing et al. (2011), and found promising results for predicting Ax-content in rainbow trout with the use of partial least squares regression model. Another study by Folkestad et al. (2008) used VIS/NIR spectroscopy and digital imaging to predict astaxanthin content in Atlantic salmon fillets. The visible spectroscopy and digital imaging data gave very high correlation with chemical reference methods for determining Ax, ranging from r=0.92 to r=0.97. Based on this research it can be argued that the results presented in this thesis should also be expected to reach high correlations between astaxanthin and spectral data. It’s possible that the high uncertainty of the HPLC

results was the reason for this, as previously mentioned, though no conclusion can be made without further research in the Ax-content of the samples.

A more promising result was the VM Lite ability to detect melanin spots in salmon fillets. The spectral profile of melanin was distinctly different from that of the reference tissue when using the controlled image protocol, though the differences was significantly decreased on the direct protocol. The largest delta value between melanin and reference tissue was given in the visible red spectra, specifically the 660 nm band. This is in accordance to Mathiassen et al. (2007) who used the red spectrum of a RGB camera to detect melanin on salmon fillets as it was hard to detect in the green and blue spectrum. However, the mentioned study did not have NIR or UV measuring capabilities whereas the results in this thesis also showed significant differences in the UV-spectrum for both imaging protocols. As the lower end of the VM Lite spectrum showed less variance between image protocols, in fact the average difference increased in the direct protocol for the 405 nm, 460 nm, and 525 nm bands compared to the direct method as reported in Chapter 4.3. Though these differences are likely caused by different backgrounds as previously discussed. There is no other previous research that describes the spectra of melanin in salmon or other salmonids as to the authors knowledge.

A clear difference in chroma was observed between melanin and reference tissue in both image protocols, suggesting that RGB detection may prove adequate for melanin detection. Though the only attempt found on this by the previously mentioned study of Mathiassen et al. (2007) had some issues with falsely detected spots. More modern multispectral imaging devices may provide a better detector for melanin spots then broadband spectrum.

5.2 Detection for loss of freshness and spoilage in head-on-gutted salmon

The loss of freshness was detected by the VM Lite prototype on salmon skin by the measured reducing reflections of the samples over time on all wavelength bands. The wavelength band that showed the most significant differences between fresh, matured, and spoiled samples was the 405 nm band. This band had also had the highest correlations with the salmon skin samples' QIM-score and microbial counts. The skin samples also showed higher absorption in the 405 nm band than the rest

of the spectrum. Absorption peaks in the 400 nm range are known as Soret peaks and are often associated with haem-containing moieties like haemoglobin and myoglobin in meats (Cozzolino & Murray, 2004; Jacob, 1991). High absorption in the 400 nm range of salmon skin was also fund by Wu et al. (2018) and suggested it was caused by methaemoglobin or metmyoglobin based on source material of Tang et al. (2004). This would make sense in pure meat or meat products as they naturally contain large quantity of these proteins, but it was doubted that haemoglobins are the only responsible factor for increased absorbance of the 405 nm range in salmon skin.

A likely explanation for the higher absorbance in the lower spectra of salmon skin has to do with the components of the skin. Salmon skin consists of three layers, the epidermis and dermis being the inner layers and an outer layer of mucus (Elliott, 2011). The mucus layer consists of glycoproteins called mucins and these proteins have been proven in some cases to have a high absorbance in the lower part of the visible spectrum (Baranowski, 2006), though spectral reflectance or absorbance of mucus in salmon or other fish is poorly reported. It was however noticed in reviews of the grayscale images (see example in Figure 4-12), that mucus on fresh salmon skin had a low reflectance of the 405 nm band compared to the skin. Salmon mucus also contains fatty acids such as the saturated fatty acids palmitic and stearic acids, monosaturated fatty acids (oleic acid) and polyunsaturated fatty acids like DHA and EPA (Dash et al., 2018; Sprague & Desbois, 2021). Similar fatty acids compositions in edible vegetable oils have showed low reflectance and high absorbance in lower parts of the visible spectrum (de Oliveira et al., 2019; Su et al., 2021). Suggesting that the components of salmon mucus can be responsible for low reflectance at 405 nm band. It is also likely that components in the epidermis and dermis of the salmon skin contributes to absorbance of this wavelength band, as it was observed that exposed epidermal skin had very low reflection in the 405 nm band compared to the scales.

The salmon scales were the most reflective component on the skin and is due to the light reflection properties of guanine crystal layers embedded in the scales, which shown to reflect light in the visible spectrum to a high degree (Levy-Lior et al., 2008). Another important component of salmon skin that contributes to reflectance are purine-pigments that is in the outermost layer of the skin. These pigments are associated with the silvery shine of immature salmon (Leclercq et

al., 2010). These facts lead to the hypothesis that correlations of QIM and microbial growth with skin reflectance spectra is due to the progressively removal of scales over time. As imaging of the HOG salmon was done each day of the experiment, the frequent handling of the salmon samples propagated the loss of scales on the skin such that the reflectance at 405 nm was lowered by exposing the epidermal layer with lower reflectance. The frequent handling of the samples had most likely contributed to faster and more severe loss of scales compared to a realistic scenario where the salmon would have been left unhandled until use. However, mechanical factors cannot be the sole factor to deterioration of the skin as autolytic, bacterial, and possibly oxidative actions will affect the skin quality and appearance over time as well. Especially one factor that was believed to effect spectral results of the abdomen images over time is from the QIM-descriptor for skin of salmon stored on ice that states yellowing near abdomen. This descriptor was added by Sveinsdottir et al. (2002) as an additional point for the skin appearance. Explanations for this discolouration of the lower abdomen is not well described in literature, but this part of the salmon contains high amounts of lipids. Hinting that peroxide products from enzymatic oxidation and hydrolyzation of lipids with endogen or bacterial enzymes may cause the yellow discolouration over time.

The creamy white colouration of the fresh salmon abdomen makes for a homogeneous-colour pallet where changes are easier to detect in the VIS-spectra, compared to the more heterogenous colouration of the dorsal area. The phenomena of yellowing of the abdominal skin can also perhaps make a connection to lipid oxidation of ice stored HOG salmon. If so, it may be possible to corelate this by the help of antioxidative tests with spectral data and predict oxidation levels of lipids in the sample.

Creating a better segmentation based on multiple classes would also help giving more accurate data. The segmentation used on the skin samples was based on just two classes, where there was the silvery skin and scales versus everything else. It might be better to separate skin and scales into different classes as it was discovered that their reflective properties are significantly different. Although including more classes would make processing of the results more complicated as the amount of data would be doubled or tripled depending on how many classes are included. A solution would be to create different classes and analyse their correlations to quality parameters, picking the best performing class for further

use. Such an attempt could be done with existing data, but it would be a time-consuming process and require further research in MSI segmentation techniques.

Difference between the QIM-score of the two storage trails was observed, where to first storage trail had a higher QIM-score than the second. Some of the reasons are most likely due to the extensive fish handling during the experiments. In storage trail one all the HOG salmon was imaged every day with VMLite and every other day with both VMLab2 and VMLite. Since imaging of the HOG-salmon required to take the fish out of the cold room and Styrofoam boxes, the salmon were exposed to higher temperatures. The regular temperature increases caused by imaging would by all likelihood lead to faster microbial growth (Sivertsvik et al., 2003), which in turn leads to faster spoilage. Since storage experiment one used two MSI devices, this would lead to a doubling of the time salmon samples was exposed to room temperature compared to days with only one imaging device. Storage trail two only used one MSI device and samples from the microbial sample pool was added to the QIM sampling after microbial analysis had been done on these samples. In practice this would mean that faster imaging and additions of lightly handled samples in storage trail two lead to lower QIM-scores and slower spoilage.

In the results of gills, an interesting factor was that both 405 nm and 850 nm (NIR) gave significant correlation ($p<0.05$) with QIM and microbial score. The NIR spectra having higher correlations with Pseudomonas spp. ($r=0.732$), total aerobic counts ($r=0.750$) and H_2S-producing bacteria ($r=0.527$) than the 405 nm spectra. On the inspection of the image spectra of gills it was clear that only the 850 nm spectra had the required reflection of gill tissue for visual inspection. The lower band waves reflected poorly off the gill and morphological traits could not be determined at 405 nm. With this it was suggested that the NIR-spectra are most suitable for quality determination of gill tissue, as this wavelength had the only significant changes in reflectance over time, seen in Figure 4-10a.

It was also noted that the average spectra of gills decreased in reflectance from fresh to matured quality and then increased in reflection to a level above fresh when reaching spoilage. A similar study by Dowlati et al. (2013) where the colour of farmed sea bream gills were measured over time showed that the changes in

redness decreased over time, while lightness and yellowness had slight increases. All the changes in colour presented in the study of Dowlati et al. (2013) was linear and is contradictory to the changes in reflectance observed for the salmon gills. The QIM descriptors for salmon gill colour (Appendix 1a) also contradicts the changes observed in the results, as it describes a change going from red or dark brown in fresh gills, to light red, pink/light brown in matured gills and finally grey brown, brown, grey or green in spoiled gills (Sveinsdottir et al., 2002). These contradictions may be explained that the HOG salmon samples used in these experiments were bled by stabbing the gill with a knife, effectively cutting the gill-arch in two. This bleeding practice led to a lot of residual blood left on the gills and rapid oxidation of haemoglobin in exposed blood may explain the reduction of reflectance. Oxidised haemoglobin (HbO_2) has a lower reflection in the 600-800 nm range a slightly higher reflection above 800nm then haemoglobin (Hb) (Dimauro & Simone, 2020; Zhao et al., 2017). The use of both cut and uncut gills may have skewed the results for both multispectral, QIM, and microbial measurements. As cut gills tended to change colour and gain higher QIM-scores faster than uncut gills.

6 Conclusion

The direct image protocol had significant differences with the control protocol caused by a difference in background and perhaps the influence of external light sources and camera shake during imaging. This led to the conclusion that using the Videometer Lite prototype directly on salmon samples leads to increased bias, in that results are affected by the person operating the device. Controlled imaging leads to no bias, but results are affected by the background material. The direct protocol needs further evaluations and measurements to reduce bias when imaging to assure similar results as to the control protocol.

The VideometerLite prototype showed to evaluate colour similarly to RGB colour measurement systems although colour value representation differed between the instruments. The results showed that the VM Lite prototype can give accurate colour representation of salmon fillets. The device also showed some potential to measure astaxanthin although more accurate data is required to affirm this.

A clear detection of melanin spots in salmon fillets was achieved using multispectral imaging and showed the possibility to discriminate between melanin and salmon muscle tissue by both spectral and coulometric information.

The spectral data from VM Lite showed good correlation with both QIM and microbial measurements of head-on-gutted salmon stored on ice. Showing the potential for using the abdominal area of the skin and the gills as indicators for estimating freshness and remaining storage time on ice. The wavelengths that gave highest correlation with the quality parameters was 405 nm for the skin and 850 nm for the gills.

7 Future perspective

As of May 2023, there are still a lot of results that can be processed out of the data that was acquired during this thesis. The spectral images of the eye region form the storage trails needs to be processed and evaluated. Statistical analysis of the multispectral data from VideometerLab2 could also be interesting to look at as it can be used to evaluate the VideometerLite prototype further.

Around 4115 multispectral images of salmon fillets and HOG-salmon was captured during the period of this thesis. This amount of data would be valuable in the creation of advanced predictor models, as it could be used to train neural network models in predicting the quality parameters with great accuracy, as has been done in similar studies (Dissing et al., 2011; Wu et al., 2018). This is in fact one of the end goals of the TraceMyFish project and future attempts will hopefully be able to utilize such models.

Further experiments within the Atlantic salmon value chain will be conducted. Salmon fillets stored in vacuum, MAP, and on ice will be measured over 21 days with a new MSI prototype that has UV-fluorescence capabilities. The effect of bleeding will be investigated also in a sperate attempt.

References

Alfnes, F., Guttormsen, A. G., Steine, G., & Kolstad, K. (2006). Consumers' Willingness to Pay for the Color of Salmon: A Choice Experiment with Real Economic Incentives. *American Journal of Agricultural Economics*, *88*(4), 1050-1061. https://doi.org/https://doi.org/10.1111/j.1467-8276.2006.00915.x

Altringham, J. D., & Ellerby, D. J. (1999). Fish swimming: patterns in muscle function. *Journal of Experimental Biology*, *202*(23), 3397-3403. https://doi.org/10.1242/jeb.202.23.3397

Amoroso, G., Elizur, A., Ventura, T., Nguyen, C., & Thu, V. (2020). *Understanding flesh colour variation in Atlantic salmon: molecular mechanisms and genetic effect*. https://www.frdc.com.au/project/2014-248

Anderson, S. (2000). Salmon Color and the Consumer. *Proceedings of the Tenth Biennial Con- ference of the International Institute of Fisheries Economics and Trade Presentations*. https://doi.org/http://localhost/files/9s1616848

Baranowski, W. J. (2006). UV-VIS spectra of intestinal mucins with change in solution concentration and pH. *Advances in Clinical and Experimental Medicine*, *15*, 253-258.

Bernardo, Y. A. A., Rosario, D. K. A., Delgado, I. F., & Conte-Junior, C. A. (2020). Fish Quality Index Method: Principles, weaknesses, validation, and alternatives—A review. *Comprehensive Reviews in Food Science and Food Safety*, *19*(5), 2657-2676. https://doi.org/10.1111/1541-4337.12600

Bjerkeng, B., Peisker, M., von Schwartzenberg, K., Ytrestøyl, T., & Åsgård, T. (2007). Digestibility and muscle retention of astaxanthin in Atlantic salmon, Salmo salar, fed diets with the red yeast Phaffia rhodozyma in comparison with synthetic formulated astaxanthin. *Aquaculture*, *269*(1), 476-489. https://doi.org/https://doi.org/10.1016/j.aquaculture.2007.04.070

Blanch-Pérez del Notario, C., López-Molina, C., Lambrechts, A., & Saeys, W. (2020). Hyperspectral system trade-offs for illumination, hardware and analysis methods: a case study of seed mix ingredient discrimination. *Journal of Spectral Imaging*, *9*(1), a1. https://doi.org/10.1255/jsi.2020.a16

Bligh, E. G., & Dyer, W. J. (1959). A RAPID METHOD OF TOTAL LIPID EXTRACTION AND PURIFICATION. *Canadian Journal of Biochemistry and Physiology*, *37*(8), 911-917. https://doi.org/10.1139/o59-099 %M 13671378

Bremner, H. (1985). A convenient, easy to use system for estimating the quality of chilled seafoods. *Fish Processing Bulletin*, *7*, 59-70.

Buchwald, M., & Jencks, W. P. (1968). Optical properties of astaxanthin solutions and aggregates. *Biochemistry*, *7*(2), 834-843.
Cantas, L., Fraser, T. W. K., Fjelldal, P. G., Mayer, I., & Sørum, H. (2011). The culturable intestinal microbiota of triploid and diploid juvenile Atlantic salmon (Salmo salar) - a comparison of composition and drug resistance. *BMC Veterinary Research*, *7*(1), 71. https://doi.org/10.1186/1746-6148-7-71
Carstensen, A. S. (2022). Personal Communication: Meeting with Videometer 15.12.2022. In M. H. Hansen (Ed.).
Carstensen, J. M., & Flom-Hansen, J. (2006). *Apparatus and Method of Recording an Image of an Object*. U. S. P. a. T. Office. https://videometer.com/wp-content/uploads/2021/08/VideometerLab-Patent.pdf
CHEN, H.-H., CHIU, E.-M., & HUANG, J.-R. (1997). Color and Gel-forming Properties of Horse Mackerel (Trachurus japonicus) as Related to Washing Conditions. *Journal of Food Science*, *62*(5), 985-991. https://doi.org/https://doi.org/10.1111/j.1365-2621.1997.tb15021.x
Cheng, J.-H., Dai, Q., Sun, D.-W., Zeng, X.-A., Liu, D., & Pu, H.-B. (2013). Applications of non-destructive spectroscopic techniques for fish quality and safety evaluation and inspection. *Trends in Food Science & Technology*, *34*(1), 18-31. https://doi.org/https://doi.org/10.1016/j.tifs.2013.08.005
CIE. (2004). *Colorimetry : technical report* (3rd edition. ed.). Commission internationale de l'éclairage.
Cooper, G. M. (2000). Actin, Myosin, and Cell Movement. In *The Cell : a molecular approach* (2nd ed.). ASM Press.
Cozzolino, D., & Murray, I. (2004). Identification of animal meat muscles by visible and near infrared reflectance spectroscopy. *LWT - Food Science and Technology*, *37*(4), 447-452. https://doi.org/https://doi.org/10.1016/j.lwt.2003.10.013
Dash, S., Das, S. K., Samal, J., & Thatoi, H. N. (2018). Epidermal mucus, a major determinant in fish health: a review. *Iran J Vet Res*, *19*(2), 72-81.
Daskalova, A. (2019). Farmed fish welfare: stress, post-mortem muscle metabolism, and stress-related meat quality changes. *International Aquatic Research*, *11*(2), 113-124. https://doi.org/10.1007/s40071-019-0230-0
de Oliveira, J. B., Michels, F. S., Silva de Pádua Melo, E., Nazário, C. E. D., Caires, A. R. L., Gonçalves, D. A., Cardoso, C. A. L., & Aragão do Nascimento, V. (2019). Data on mineral composition, fatty acids, oxidative stability, UV-VIS spectra and fluorescence emission of the Dersani® and Sunflower® oils used as a cicatrizing agent. *Data in Brief*, *26*, 104427. https://doi.org/https://doi.org/10.1016/j.dib.2019.104427
Dimauro, G., & Simone, L. (2020). Novel Biased Normalized Cuts Approach for the Automatic Segmentation of the Conjunctiva. *Electronics*, *9*, 997. https://doi.org/10.3390/electronics9060997

Dissing, B. S., Nielsen, M. E., Ersbøll, B. K., & Frosch, S. (2011). Multispectral Imaging for Determination of Astaxanthin Concentration in Salmonids. *PLOS ONE*, *6*(5), e19032. https://doi.org/10.1371/journal.pone.0019032

Dowlati, M., Mohtasebi, S. S., Omid, M., Razavi, S. H., Jamzad, M., & de la Guardia, M. (2013). Freshness assessment of gilthead sea bream (Sparus aurata) by machine vision based on gill and eye color changes. *Journal of food engineering*, *119*(2), 277-287. https://doi.org/https://doi.org/10.1016/j.jfoodeng.2013.05.023

Downey, G. (1996). Non-invasive and non-destructive percutaneous analysis of farmed salmon flesh by near infra-red spectroscopy. *Food Chemistry*, *55*(3), 305-311. https://doi.org/https://doi.org/10.1016/0308-8146(95)00118-2

Elliott, D. G. (2011). THE SKIN | Functional Morphology of the Integumentary System in Fishes. In A. P. Farrell (Ed.), *Encyclopedia of Fish Physiology* (pp. 476-488). Academic Press. https://doi.org/https://doi.org/10.1016/B978-0-12-374553-8.00108-8

ElMasry, G., Mandour, N., Al-Rejaie, S., Belin, E., & Rousseau, D. (2019). Recent Applications of Multispectral Imaging in Seed Phenotyping and Quality Monitoring-An Overview. *Sensors (Basel)*, *19*(5). https://doi.org/10.3390/s19051090

ElMasry, G., Sun, D.-W., & Allen, P. (2011). Non-destructive determination of water-holding capacity in fresh beef by using NIR hyperspectral imaging. *Food Research International*, *44*(9), 2624-2633. https://doi.org/https://doi.org/10.1016/j.foodres.2011.05.001

Emborg, J., Laursen, B. G., Rathjen, T., & Dalgaard, P. (2002). Microbial spoilage and formation of biogenic amines in fresh and thawed modified atmosphere-packed salmon (Salmo salar) at 2°C [Article]. *Journal of Applied Microbiology*, *92*(4), 790-799. https://doi.org/10.1046/j.1365-2672.2002.01588.x

Erikson, U., & Misimi, E. (2008). Atlantic Salmon Skin and Fillet Color Changes Effected by Perimortem Handling Stress, Rigor Mortis, and Ice Storage. *Journal of Food Science*, *73*(2), C50-C59. https://doi.org/https://doi.org/10.1111/j.1750-3841.2007.00617.x

Evans, J. D. (1996). *Straightforward statistics for the behavioral sciences*. Thomson Brooks/Cole Publishing Co.

FAO. (2022). The State of World Fisheries and Aquaculture 2022. Towards Blue Transformation. . *Rome, FAO*. https://doi.org/10.4060/cc0461en

FAO/WHO. (2011). *Report of the Joint FAO/WHO Expert Consultation on the Risks and Benefits of Fish consumption. Rome, 25-29 January 2010*. FAO, Rome (Italy).

Fogarty, C., Whyte, P., Brunton, N., Lyng, J., Smyth, C., Fagan, J., & Bolton, D. (2019). Spoilage indicator bacteria in farmed Atlantic salmon (Salmo salar) stored on ice for 10 days. *Food Microbiology*,

77, 38-42. https://doi.org/https://doi.org/10.1016/j.fm.2018.08.001
Folkestad, A., Wold, J. P., Rørvik, K.-A., Tschudi, J., Haugholt, K. H., Kolstad, K., & Mørkøre, T. (2008). Rapid and non-invasive measurements of fat and pigment concentrations in live and slaughtered Atlantic salmon (Salmo salar L.). *Aquaculture*, *280*(1), 129-135. https://doi.org/https://doi.org/10.1016/j.aquaculture.2008.04.037
Freitas, J., Vaz-Pires, P., & Câmara, J. S. (2021). Quality Index Method for fish quality control: Understanding the applications, the appointed limits and the upcoming trends. *Trends in Food Science & Technology*, *111*, 333-345. https://doi.org/https://doi.org/10.1016/j.tifs.2021.03.011
Geesink, G. H., Kuchay, S., Chishti, A. H., & Koohmaraie, M. (2006). μ-Calpain is essential for postmortem proteolysis of muscle proteins1,2. *Journal of Animal Science*, *84*(10), 2834-2840. https://doi.org/10.2527/jas.2006-122
Gram, L., & Huss, H. H. (1996). Microbiological spoilage of fish and fish products [Article]. *International Journal of Food Microbiology*, *33*(1), 121-137. https://doi.org/10.1016/0168-1605(96)01134-8
Gram, L., & Huss, H. H. (2000). Fresh and processed fish and shellfish. In *The microbiological safety and quality of food* (pp. 472-506). Aspen Publishers.
Hannisdal, A., & Hemmer, E. (2017). *Kjøtt-teknologi. Kompendium*.
Harmon, K. J., Bolinger, M. T., & Rodnick, K. J. (2011). Carbohydrate energy reserves and effects of food deprivation in male and female rainbow trout [Article]. *Comparative Biochemistry and Physiology - A Molecular and Integrative Physiology*, *158*(4), 423-431. https://doi.org/10.1016/j.cbpa.2010.11.017
Hemmer, E. (1997). *Kjøtt-teknologi*. Tapir.
Herrera-Ramírez, J., Vilaseca, M., & Pujol, J. (2014). Portable multispectral imaging system based on light-emitting diodes for spectral recovery from 370 to 1630 nm. *Applied Optics*, *53*(14), 3131-3141. https://doi.org/10.1364/AO.53.003131
Hicks, C. C., Cohen, P. J., Graham, N. A. J., Nash, K. L., Allison, E. H., D'Lima, C., Mills, D. J., Roscher, M., Thilsted, S. H., Thorne-Lyman, A. L., & MacNeil, M. A. (2019). Harnessing global fisheries to tackle micronutrient deficiencies. *Nature*, *574*(7776), 95-98. https://doi.org/10.1038/s41586-019-1592-6
Hirschler, R. (2016). CIE Method of Assessing Daylight Simulators. In M. R. Luo (Ed.), *Encyclopedia of Color Science and Technology* (pp. 157-165). Springer New York. https://doi.org/10.1007/978-1-4419-8071-7_328
Hirschler, R., Oliveira, D. F., & Lopes, L. C. (2011). Quality of the daylight sources for industrial colour control. *Coloration Technology*, *127*(2), 88-100. https://doi.org/https://doi.org/10.1111/j.1478-4408.2011.00283.x

Hossain, K. Z. (2022). Melanin: Definition, Cause and Its Role in Atlantic Salmon-A Review. *American Journal of Aquaculture and Animal Science*, *1*(1), 11-14. https://doi.org/10.54536/ajaas.v1i1.851
Hovda, M. B., Fontanillas, R., McGurk, C., Obach, A., & Rosnes, J. T. (2012). Seasonal variations in the intestinal microbiota of farmed Atlantic salmon (Salmo salar L.) [Article]. *Aquaculture Research*, *43*(1), 154-159. https://doi.org/10.1111/j.1365-2109.2011.02805.x
Huss, H. (1976). Konsumfisk - biologi, teknologi, kvalitet og holdbarhed. *Dansk Get. Tidsskr.*(59), 165-175.
Huss, H., H. (1995). *Quality and quality changes in fresh fish*. FAO Fisheries Technical Paper.
Jacob, K. (1991). Prophyrins. In E. Heftmann (Ed.), *Chromatography, 5th edition* (5 ed., Vol. 51B, pp. 336-359). Elesevier.
Jiang, Q., Zhang, M., Mujumdar, A. S., & Wang, D. (2023). Non-destructive quality determination of frozen food using NIR spectroscopy-based machine learning and predictive modelling [Article]. *Journal of food engineering*, *343*, Article 111374. https://doi.org/10.1016/j.jfoodeng.2022.111374
Johnston, I. A., Alderson, R., Sandham, C., Dingwall, A., Mitchell, D., Selkirk, C., Nickell, D., Baker, R., Robertson, B., Whyte, D., & Springate, J. (2000). Muscle fibre density in relation to the colour and texture of smoked Atlantic salmon (Salmo salar L.) [Article]. *Aquaculture*, *189*(3-4), 335-349. https://doi.org/10.1016/S0044-8486(00)00373-2
Johnston, I. A., Li, X., Vieira, V. L. A., Nickell, D., Dingwall, A., Alderson, R., Campbell, P., & Bickerdike, R. (2006). Muscle and flesh quality traits in wild and farmed Atlantic salmon. *Aquaculture*, *256*(1), 323-336. https://doi.org/https://doi.org/10.1016/j.aquaculture.2006.02.048
Karatas, T. (2018). Effect of short-term starvation on serum metabolites, antioxidant enzymes and endogenous reserves of rainbow trout, Oncorhynchus mykiss. *Pakistan Journal of Zoology*, *50*(5).
Kidane, D. G., & Brækkan, E. H. (2021). Global Seafood Demand Growth Differences across Regions, Income Levels, and Time. *Marine resource economics*, *36*(3), 289-305. https://doi.org/10.1086/714122
Kim, S. (2021). Cross-bridge Cycle. https://app.biorender.com/biorender-templates/figures/all/t-6079e4ef7103ca00a005857a-cross-bridge-cycle
Komolka, K., Bochert, R., Franz, G. P., Kaya, Y., Pfuhl, R., & Grunow, B. (2020). Determination and Comparison of Physical Meat Quality Parameters of Percidae and Salmonidae in Aquaculture. *Foods*, *9*(4), 388. https://www.mdpi.com/2304-8158/9/4/388
Koteng, D., F. (1992). Markedsundersøkelse, norsk laks. Prosjekt God Fisk. *Fiskerinaeringsens Landsforening (FNL)*.
Leclercq, E., Dick, J. R., Taylor, J. F., Bell, J. G., Hunter, D., & Migaud, H. (2010). Seasonal variations in skin pigmentation and flesh quality of atlantic salmon (Salmo salar L.): Implications for quality

management [Article]. *Journal of Agricultural and Food Chemistry*, *58*(11), 7036-7045. https://doi.org/10.1021/jf100723b
Lerfall, J., Bendiksen, E. Å., Olsen, J. V., Morrice, D., & Østerlie, M. (2016). A comparative study of organic- versus conventional farmed Atlantic salmon. I. Pigment and lipid content and composition, and carotenoid stability in ice-stored fillets. *Aquaculture*, *451*, 170-177. https://doi.org/https://doi.org/10.1016/j.aquaculture.2015.09.013
Lerfall, J., Jakobsen, A. N., Tsakanikas, P., Guðjónsdóttir, M., & Sveinsdóttir, H. I. (2023). TraceMyFish D2.2 User requirement specification (v2.0). https://doi.org/10.5281/zenodo.7793470
Levy-Lior, A., Pokroy, B., Levavi-Sivan, B., Leiserowitz, L., Weiner, S., & Addadi, L. (2008). Biogenic Guanine Crystals from the Skin of Fish May Be Designed to Enhance Light Reflectance. *Crystal Growth & Design*, *8*(2), 507-511. https://doi.org/10.1021/cg0704753
Liu, C., Liu, W., Lu, X., Chen, W., Yang, J., & Zheng, L. (2016). Potential of multispectral imaging for real-time determination of colour change and moisture distribution in carrot slices during hot air dehydration. *Food Chemistry*, *195*, 110-116. https://doi.org/https://doi.org/10.1016/j.foodchem.2015.04.145
Lunestad, B. (2003). Absence of Nematodes in Farmed Atlantic Salmon (Salmo salar L.) in Norway. *Journal of food protection*, *66*, 122-124. https://doi.org/10.4315/0362-028X-66.1.122
Mackintosh, J. A. (2001). The Antimicrobial Properties of Melanocytes, Melanosomes and Melanin and the Evolution of Black Skin. *Journal of Theoretical Biology*, *211*(2), 101-113. https://doi.org/https://doi.org/10.1006/jtbi.2001.2331
Manson, J. E., Cook, N. R., Lee, I.-M., Christen, W., Bassuk, S. S., Mora, S., Gibson, H., Albert, C. M., Gordon, D., Copeland, T., D'Agostino, D., Friedenberg, G., Ridge, C., Bubes, V., Giovannucci, E. L., Willett, W. C., & Buring, J. E. (2018). Marine n−3 Fatty Acids and Prevention of Cardiovascular Disease and Cancer. *New England Journal of Medicine*, *380*(1), 23-32. https://doi.org/10.1056/NEJMoa1811403
Mathiassen, J. R., Misimi, E., & Skavhaug, A. (2007, 5-7 Sept. 2007). A Simple Computer Vision Method for Automatic Detection of Melanin Spots in Atlantic Salmon Fillets. International Machine Vision and Image Processing Conference (IMVIP 2007),
Matthews, S. J., Ross, N. W., Lall, S. P., & Gill, T. A. (2006). Astaxanthin binding protein in Atlantic salmon. *Comparative Biochemistry and Physiology Part B: Biochemistry and Molecular Biology*, *144*(2), 206-214. https://doi.org/https://doi.org/10.1016/j.cbpb.2006.02.007
Mozaffarian, D., & Wu, J. H. Y. (2011). Omega-3 Fatty Acids and Cardiovascular Disease. *Journal of the American College of Cardiology*, *58*(20), 2047-2067. https://doi.org/doi:10.1016/j.jacc.2011.06.063
Møretrø, T., Moen, B., Heir, E., Hansen, A. Å., & Langsrud, S. (2016). Contamination of salmon fillets and processing plants with spoilage

bacteria. *International Journal of Food Microbiology*, *237*, 98-108. https://doi.org/https://doi.org/10.1016/j.ijfoodmicro.2016.08.016
Mørkøre, T. (2017). *Mørke flekker i laksefilet - kunnskapsstatus*. https://doi.org/10.13140/RG.2.2.12843.13608
Nanton, D. A., Vegusdal, A., Rørå, A. M. B., Ruyter, B., Baeverfjord, G., & Torstensen, B. E. (2007). Muscle lipid storage pattern, composition, and adipocyte distribution in different parts of Atlantic salmon (Salmo salar) fed fish oil and vegetable oil. *Aquaculture*, *265*(1), 230-243. https://doi.org/https://doi.org/10.1016/j.aquaculture.2006.03.053
Nilsen, H., Esaiassen, M., Heia, K., & Sigernes, F. (2002). Visible/Near-Infrared Spectroscopy: A New Tool for the Evaluation of Fish Freshness? *Journal of Food Science*, *67*(5), 1821-1826. https://doi.org/https://doi.org/10.1111/j.1365-2621.2002.tb08729.x
NMKL. (2006). Kimtal og specifikke fordær-velsesbakterier i fisk og fiskevarer. NMKL-metode Nr. 184 https://www.nmkl.org/product/aerobic-count-and-specific-spoilage-organisms-in-fish-and-fish-products/
Nychas, G. J. E., Lerfall, J., Sveinsdóttir, H. I., Lytou, A., Kobbenes, S. M. M., Jakobsen, A. N., Fengou, L., Tsakanikas, P., Schultz, N., Genio, A., & Guðjónsdóttir, M. (2023). TraceMyFish D2.4 Pilot Design and Piloting plan (v2.0). *Zendo*. https://doi.org/10.5281/zenodo.7793472
Odden, K. (2020). *Prosjekt Japan 1985-1990: Hvordan norsk laks ble solgt som sushi på det japanske markedet* NTNU]. NTNU Open. https://hdl.handle.net/11250/2775537
Ojima, K. (2019). Myosin: Formation and maintenance of thick filaments. *Animal Science Journal*, *90*(7), 801-807. https://doi.org/10.1111/asj.13226
Parlapani, F. F., & Boziaris, I. S. (2016). Monitoring of spoilage and determination of microbial communities based on 16S rRNA gene sequence analysis of whole sea bream stored at various temperatures [Article]. *LWT*, *66*, 553-559. https://doi.org/10.1016/j.lwt.2015.11.007
Pathare, P. B., Opara, U. L., & Al-Said, F. A. J. (2013). Colour Measurement and Analysis in Fresh and Processed Foods: A Review [Review]. *Food and Bioprocess Technology*, *6*(1), 36-60. https://doi.org/10.1007/s11947-012-0867-9
Polvi, S. M., & Ackman, R. G. (1992). Atlantic Salmon (Salmo salar) Muscle Lipids and Their Response to Alternative Dietary Fatty Acid Sources [Article]. *Journal of Agricultural and Food Chemistry*, *40*(6), 1001-1007. https://doi.org/10.1021/jf00018a018
Qin, J., Chao, K., Kim, M. S., Lu, R., & Burks, T. F. (2013). Hyperspectral and multispectral imaging for evaluating food safety and quality. *Journal of food engineering*, *118*(2), 157-171. https://doi.org/10.1016/j.jfoodeng.2013.04.001

Reddi, P. K., Constantinides, S. M., & Dymsza, H. A. (1972). CATHEPTIC ACTIVITY OF FISH MUSCLE. *Journal of Food Science*, *37*(5), 643-648. https://doi.org/https://doi.org/10.1111/j.1365-2621.1972.tb02716.x

Schultz, N., Genio, A., Carstensen, A. S., & M., C. J. (2023). *TraceMyFish D3.1 Handheld Sensor Prototype*.

Setchell, J. S. (2012). 4 - Colour description and communication. In J. Best (Ed.), *Colour Design (Second Edition)* (pp. 99-129). Woodhead Publishing. https://doi.org/https://doi.org/10.1016/B978-0-08-101270-3.00004-7

Sivertsvik, M., Rosnes, J. T., & Kleiberg, G. H. (2003). Effect of Modified Atmosphere Packaging and Superchilled Storage on the Microbial and Sensory Quality of Atlantic Salmon (Salmo salar) Fillets. *Journal of Food Science*, *68*(4), 1467-1472. https://doi.org/10.1111/j.1365-2621.2003.tb09668.x

Skrede, G., Risvik, E., Huber, M., Enersen, G., & BlÜMlein, L. (1990). Developing a Color Card for Raw Flesh of Astaxanthin-fed Salmon [Article]. *Journal of Food Science*, *55*(2), 361-363. https://doi.org/10.1111/j.1365-2621.1990.tb06763.x

Sotelo, C. G., Piñeiro, C., Pérez-Martín, R. I., & Gallardo, J. M. (2000). Analysis of fish and squid myofibrillar proteins by capillary sodium dodecyl sulfate gel electrophoresis: actin and myosin quantification. *European Food Research and Technology*, *211*(6), 443-448. https://doi.org/10.1007/s002170000176

Sprague, M., & Desbois, A. P. (2021). Fatty acid and lipid class composition in cutaneous mucus of Atlantic salmon, Salmo salar (L.). *Aquaculture Research*, *52*(12), 6808-6813. https://doi.org/https://doi.org/10.1111/are.15512

SSB. (2020, 29.10.2020). *Akvakultur*. Retrieved 08.09 from https://www.ssb.no/jord-skog-jakt-og-fiskeri/statistikker/fiskeoppdrett

Stonehouse, W. (2014). Does Consumption of LC Omega-3 PUFA Enhance Cognitive Performance in Healthy School-Aged Children and throughout Adulthood? Evidence from Clinical Trials. *Nutrients*, *6*(7), 2730-2758. https://www.mdpi.com/2072-6643/6/7/2730

Su, N., Pan, F., Wang, L., & Weng, S. (2021). Rapid Detection of Fatty Acids in Edible Oils Using Vis-NIR Reflectance Spectroscopy with Multivariate Methods. *Biosensors*, *11*(8), 261. https://www.mdpi.com/2079-6374/11/8/261

Sveinsdottir, K., Martinsdottir, E., Hyldig, G., Jørgensen, B., & Kristbergsson, K. (2002). Application of Quality Index Method (QIM) scheme in shelf-life study of farmed Atlantic salmon (Salmo salar) [Article]. *Journal of Food Science*, *67*(4), 1570-1579. https://doi.org/10.1111/j.1365-2621.2002.tb10324.x

Tang, J., Faustman, C., & Hoagland, T. A. (2004). Krzywicki Revisited: Equations for Spectrophotometric Determination of Myoglobin Redox Forms in Aqueous Meat Extracts. *Journal of Food Science*, *69*(9),

C717-C720. https://doi.org/https://doi.org/10.1111/j.1365-2621.2004.tb09922.x
TMF. (N.D.). *Project Summary*. Retrieved 15.03.2023 from https://tracemyfish.hi.is/about/
Torrissen, O. J. (1989). Pigmentation of salmonids: Interactions of astaxanthin and canthaxanthin on pigment deposition in rainbow trout. *Aquaculture*, *79*(1), 363-374. https://doi.org/https://doi.org/10.1016/0044-8486(89)90478-X
Torrissen, O. J., Christiansen, R., StruksnÆS, G., & Estermann, R. (1995). Astaxanthin deposition in the flesh of Atlantic Salmon, Salmo salar L., in relation to dietary astaxanthin concentration and feeding period [Article]. *Aquaculture Nutrition*, *1*(2), 77-84. https://doi.org/10.1111/j.1365-2095.1995.tb00022.x
Torrissen, O. J., Hardy, R. W., & Shearer, K. D. (1988). Pigmentation of Salmonids–Carotenoid Deposition and Metabolism. *Aquatic Sciences*, *1*(2), 209-225.
Tryfinopoulou, P., Tsakalidou, E., & Nychas, G. J. E. (2002). Characterization of Pseudomonas spp. associated with spoilage of gilt-head sea bream stored under various conditions [Article]. *Applied and Environmental Microbiology*, *68*(1), 65-72. https://doi.org/10.1128/AEM.68.1.65-72.2002
Vecchi, M., Glinz, E., Meduna, V., & Schiedt, K. (1987). HPLC separation and determination of astacene, semiastacene, astaxanthin, and other keto-carotenoids. *Journal of High Resolution Chromatography*, *10*(6), 348-351. https://doi.org/https://doi.org/10.1002/jhrc.1240100606
Viera, I., Pérez-Gálvez, A., & Roca, M. (2018). Bioaccessibility of marine carotenoids [Review]. *Marine Drugs*, *16*(10), Article 397. https://doi.org/10.3390/md16100397
Weatherley, A., Gill, H., & Rogers, S. (1979). Growth dynamics of muscle fibres, dry weight, and condition in relation to somatic growth rate in yearling rainbow trout (Salmo gairdneri). *Canadian Journal of Zoology*, *57*(12), 2385-2392.
Wu, T., Zhong, N., & Yang, L. (2018). Application of VIS/NIR Spectroscopy and SDAE-NN Algorithm for Predicting the Cold Storage Time of Salmon [Article]. *Journal of Spectroscopy*, *2018*, Article 7450695. https://doi.org/10.1155/2018/7450695
Xie, J., Zhang, Z., Yang, S.-P., Cheng, Y., & Qian, Y.-F. (2018). Study on the spoilage potential of Pseudomonas fluorescens on salmon stored at different temperatures. *Journal of Food Science and Technology*, *55*(1), 217-225. https://doi.org/10.1007/s13197-017-2916-x
Yamashita, M., & Konagaya, S. (1990). Participation of Cathepsin L into Extensive Softening of the Muscle of Chum Salmon Caught during Spawning Migration. *NIPPON SUISAN GAKKAISHI*, *56*(8), 1271-1277. https://doi.org/10.2331/suisan.56.1271
Yesilayer, N. (2020). Comparison of Flesh Colour Assessment Methods for Wild Brown Trout (Salmo trutta macrostigma), Farmed Rainbow

Trout (Oncorhynchus mykiss) and Farmed Atlantic Salmon (Salmo salar). *Pakistan Journal of Zoology*, *52*(3), 1007.
Ytrestøyl, T., Dikiy, A., Shumilina, E., Bæverfjord, G., Krasnov, A., Ciampa, A., Hatlen, B., Østby, T.-K., Mira, M. B., Dessen, J.-E., Rørvik, K.-A., & Ruyter, B. (2019). *Effekt av fôr, temperatur og stress på pigmentering i laks* (24/2019). https://www.fhf.no/prosjekter/prosjektbasen/901271/
Ytrestøyl, T., Struksnæs, G., Rørvik, K. A., Koppe, W., & Bjerkeng, B. (2006). Astaxanthin digestibility as affected by ration levels for Atlantic salmon, Salmo salar [Article]. *Aquaculture*, *261*(1), 215-224. https://doi.org/10.1016/j.aquaculture.2006.06.046
Zhao, Y., Qiu, L., Sun, Y., Huang, C., & Li, T. (2017). Optimal hemoglobin extinction coefficient data set for near-infrared spectroscopy. *Biomedical Optics Express*, *8*(11), 5151-5159. https://doi.org/10.1364/BOE.8.005151
Zheng, Q., Wang, H. H., & Shogren, J. F. (2021). Fishing or aquaculture? Chinese consumers' stated preference for the growing environment of salmon through a choice experiment and the consequentiality effect [Article]. *Marine resource economics*, *36*(1), 23-41. https://doi.org/10.1086/711385
Aas, T. S., Åsgård, T., & Ytrestøyl, T. (2022). Utilization of feed resources in the production of Atlantic salmon (Salmo salar) in Norway: An update for 2020. *Aquaculture Reports*, *26*, 101316. https://doi.org/https://doi.org/10.1016/j.aqrep.2022.101316

Appendices

Appendix 1a: QIM scoring scheme (Norwegian)

Appendix 1b: QIM prediction scheme

Appendix 2: Measured SalmoFan™ colour values

Appendix 3: Astaxanthin concentrations

Appendix 4: Microbial and spectral correlation values

Appendix 1a: QIM scoring scheme (Norwegian)

Kvalitetsindeksmetoden (QIM) skjema for oppdrettet laks

Kvalitetsparameter		Beskrivelse	Poeng
Skinn	Farge/ utseende	Perlemorskinnende over hele skinnet	0
		Redusert perlemorskinn	1
		Fisken er gulaktig, særlig nær bukhulen	2
	Slim	Klart, ikke klumpet	0
		Melkeaktig, klumpet	1
		Gult og klumpet	2
	Lukt	Frisk, tangaktig, nøytral	0
		Agurk, metall, høy	1
		Sur, kjøkkenklut	2
		Råtten	3
	Teksture	I rigor	0
		Merke etter fingertrykk forsvinner hurtig	1
		Fingertrykk etterlater merke i over 3 sekunder	2
Øyne	Pupiller	Klare, mørke, metallskinnende	0
		Mørk grå	1
		Matt, grå	2
	Form	Konveks	0
		Flat	1
		Innsunket	2
Gjeller	Farge	Rød/mørk brun	0
		Blek rød, rosa/lysebrun	1
		Gråbrun, brun, grå, grønn	2
	Slim	Klart, transparent	0
		Melkeaktig, klumpet	1
		Brunt, klumpet	2
	Lukt	Frisk, tangaktig	0
		Metall, agurk	1
		Sur, muggen	2
		Råtten	3
Bukhule	Blod i bukhule	Blodet er rødt / ikke blod	0
		Blodet er mer brunt og gulaktig	1
	Lukt	Nøytral	0
		Agurk, melon	1
		Sur, minner om fermentering	2
		Råtten / råtten kål	3
Kvalitetsindeks			0-24

Appendix 1b: QIM prediction scheme

Oppdrettslaks

Kvalitetsindeks = 0,692 x dager i is + 1,57

(R^2 = 0,953)

Kvalitets-indeks (QIM)	Lagringstid i is (dager)	Rest-holdbarhets-tid (dager)
1	0	20
2	1	19
3	3	17
4	4	16
5	6	14
6	7	13
7	9	11
8	10	10
9	11	9
10	13	7
11	14	6
12	16	4
13	17	3
14	19	1
15	20	0

Taken from:

Martinsdóttir, E., Sveinsdóttir, K., Luten, J., Schelvis-Smit, R., Hyldig, G. (2001) *Sensorisk bedømmelse av fisk med fokus på ferskhet.* QIM Eurofish.

Appendix 2: Measured SalmoFan™ colour values

Chroma values of SalmoFan™ card 21 to 29 is presented in Table Appendix 2-1, chroma values of SalmoFan™ cards outside the presented range were of no interest as all salmon fillet samples chroma values was within the presented range.

Table Appendix 2-1: Chroma values of SalmoFan™ card 21-29, taken with DigiEye and VideometerLite instruments.

SalmoFan Colour card value	DigiEye SalmoFan C*-values	VMLite SalmoFan C*-values
21	41,99	47,02
22	42,86	48,83
23	44,55	50,16
24	45,66	51,99
25	49,15	55,07
26	50,92	55,41
27	54,44	59,24
28	55,70	60,37
29	57,15	61,07

Appendix 3: Astaxanthin concentrations

Table Appendix 3-1 Results of astaxanthin concentrations (mg/Kg) of salmon fillet samples.

Sample ID	Astaxanthin concentration (mg/Kg)
1	NA
2	1,79
3	1,91
4	1,85
5	1,90
6	2,15
7	1,99
8	2,05
9	2,10
10	1,51
11	1,59
12	1,76
13	1,65
14	2,08
15	1,59
16	1,50
17	1,38
18	2,02
19	1,94
20	1,71

Calculations:

RF = 179

Dilution factor = 25

$$\frac{Area\ Ax\ x\ Dilution\ factor}{Sample\ weight(g)\ x\ RF}$$

Appendix 4: Microbial and spectral correlation values

Table appendix 4-1: Pearson correlation values between *Pseudomonas ssp*. (Psd) (log CFU/skin or gram) and mean reflectance values of each wavelength band (%). P-values indicate significance level of the correlations. * Marks significance at the p<0.05 level, ** marks significance at p<0.01 level.

Region	n=	Psd vs 405nm	Psd vs 460nm	Psd vs 525nm	Psd vs 590nm	Psd vs 621nm	Psd vs 660nm	Psd vs 850nm
Skins, R3	12	-0,437	0,186	0,299	0,398	0,419	0,436	0,492
p-value		0,156	0,562	0,345	0,2	0,176	0,157	0,104
Skins, R4	12	-,738**	-0,275	-0,304	-0,201	-0,063	-0,009	-0,036
p-value		0,006	0,387	0,338	0,530	0,846	0,978	0,911
Skins, R5	12	-,774**	-0,541	-0,519	-0,405	-0,288	-0,248	-0,334
p-value		0,003	0,069	0,084	0,192	0,363	0,437	0,289
Gills	22	-,498*	0,345	,478*	,523*	0,231	,474*	,732**
p-value		0,018	0,115	0,024	0,012	0,301	0,026	0,000

Table appendix 4-2: Pearson correlation values between Total aerobic plate count (APC) (log CFU/skin or gram) and mean reflectance values of each wavelength band (%). P-values indicate significance level of the correlations. * Marks significance at the p<0.05 level, ** marks significance at p<0.01 level.

Region	n=	Total APC vs 405nm	Total APC vs 460nm	Total APC vs 525nm	Total APC vs 590nm	Total APC vs 621nm	Total APC vs 660nm	Total APC vs 850nm
Skins, R3	12	0,093	-0,313	-0,311	-0,305	-0,347	-0,341	-0,305
p-value		0,774	0,322	0,325	0,335	0,270	0,278	0,334
Skins, R4	12	-0,625*	-0,220	-0,139	-0,092	-0,017	-0,009	-0,127
p-value		0,030	0,493	0,667	0,776	0,958	0,978	0,694
Skins, R5	12	-0,543	-0,367	-0,328	-0,274	-0,175	0,121	-0,079
p-value		0,068	0,240	0,299	0,389	0,587	0,707	0,807
Gills	22	-,455*	0,339	,476*	,517*	0,223	,469*	,750**
p-value		0,033	0,123	0,025	0,014	0,318	0,028	0,000

Table appendix 4-3: Pearson correlation values between H_2S-producing bacteria (H_2S) (log CFU/skin or gram) and mean reflectance values of each wavelength band (%). P-values indicate significance level of the correlations. * Marks significance at the p<0.05 level, ** marks significance at p<0.01 level.

Region	n=	H_2S-pro. vs 405nm	H_2S-pro vs 460nm	H_2S-pro vs 525nm	H_2S-pro vs 590nm	H_2S-pro vs 621nm	H_2S-pro vs 660nm	H_2S-pro vs 850nm
Skins, R3	12	-0,514	0,082	0,208	0,319	0,338	0,363	0,424
p-value		0,087	0,801	0,517	0,312	0,282	0,246	0,169
Skins, R4	12	-,634*	-0,180	-0,217	-0,120	0,011	0,062	0,026
p-value		0,027	0,576	0,498	0,709	0,973	0,848	0,935
Skins, R5	12	-,719**	-0,504	-0,479	-0,361	-0,260	-0,223	-0,363
p-value		0,008	0,095	0,115	0,249	0,414	0,485	0,246
Gills	22	-,504*	0,180	0,374	0,395	0,073	0,303	,527*
p-value		0,017	0,424	0,087	0,069	0,748	0,171	0,012

Table appendix 4-4: Pearson correlation values between lactic acid producing bacteria (MRS) (log CFU/skin or gram) and mean reflectance values of each wavelength band (%). P-values indicate significance level of the correlations. * Marks significance at the p<0.05 level, ** marks significance at p<0.01 level.

Region	n=	MRS vs 405nm	MRS vs 460nm	MRS vs 525nm	MRS vs 590nm	MRS vs 621nm	MRS vs 660nm	MRS vs 850nm
Skins, R3	12	-0,287	0,053	0,075	0,190	0,175	0,174	0,162
p-value		0,366	0,870	0,816	0,554	0,587	0,589	0,614
Skins, R4	12	-0,386	0,057	0,016	0,145	0,235	0,249	0,151
p-value		0,215	0,860	0,960	0,652	0,461	0,435	0,641
Skins, R5	12	-0,318	0,004	0,014	0,158	0,206	0,205	0,038
p-value		0,314	0,990	0,965	0,623	0,521	0,523	0,908
Gills	22	-,607**	-0,071	-0,066	0,024	-0,075	0,115	0,349
p-value		0,003	0,754	0,770	0,917	0,741	0,611	0,111

Table appendix 4-5: Pearson correlation values between Aerobic psychrotrophic bacteria (LH) (log CFU/skin or gram) and mean reflectance values of each wavelength band (%). P-values indicate significance level of the correlations. * Marks significance at the p<0.05 level, ** marks significance at p<0.01 level.

Region	n=	LH vs 405nm	LH vs 460nm	LH vs 525nm	LH vs 590nm	LH vs 621nm	LH vs 660nm	LH vs 850nm
Skins, R3	12	0,088	-0,349	-0,349	-0,350	-0,382	-0,379	-0,330
p-value		0,786	0,266	0,266	0,265	0,221	0,225	0,296
Skins, R4	12	,614*	0,180	0,112	0,059	-0,011	-0,031	-0,126
p-value		0,034	0,575	0,729	0,855	0,972	0,925	0,696
Skins, R5	12	0,513	0,299	0,259	0,206	0,107	0,055	-0,113
p-value		0,088	0,345	0,416	0,522	0,740	0,866	0,727
Gills	22	-,627**	0,193	0,330	0,378	0,088	0,342	,616**
p-value		0,002	0,390	0,133	0,083	0,696	0,119	0,002

Table appendix 4-6: Pearson correlation values between Aerobic psychrotrophic bacteria (LH) (log CFU/skin or gram) and Qim-score of HOG salmon over days on ice (%). P-values indicate significance level of the correlations. * Marks significance at the p<0.05 level, ** marks significance at p<0.01 level.

Region	QIM vs Psd	QIM vs (APC)	QIM vs (H2S)	QIM vs MRS	QIM vs LH (Psychotrop. APC)
Skins	0,974**	0,958**	0,964**	0,607	0,941**
p-verdi skins	<0.001	<0.001	<0.001	0.063	<0.001
Gills	0,812**	0,815**	0,92**	0,475	0,978**
p-verdi gills	0,014	0,014	0,001	0,282	<0,001

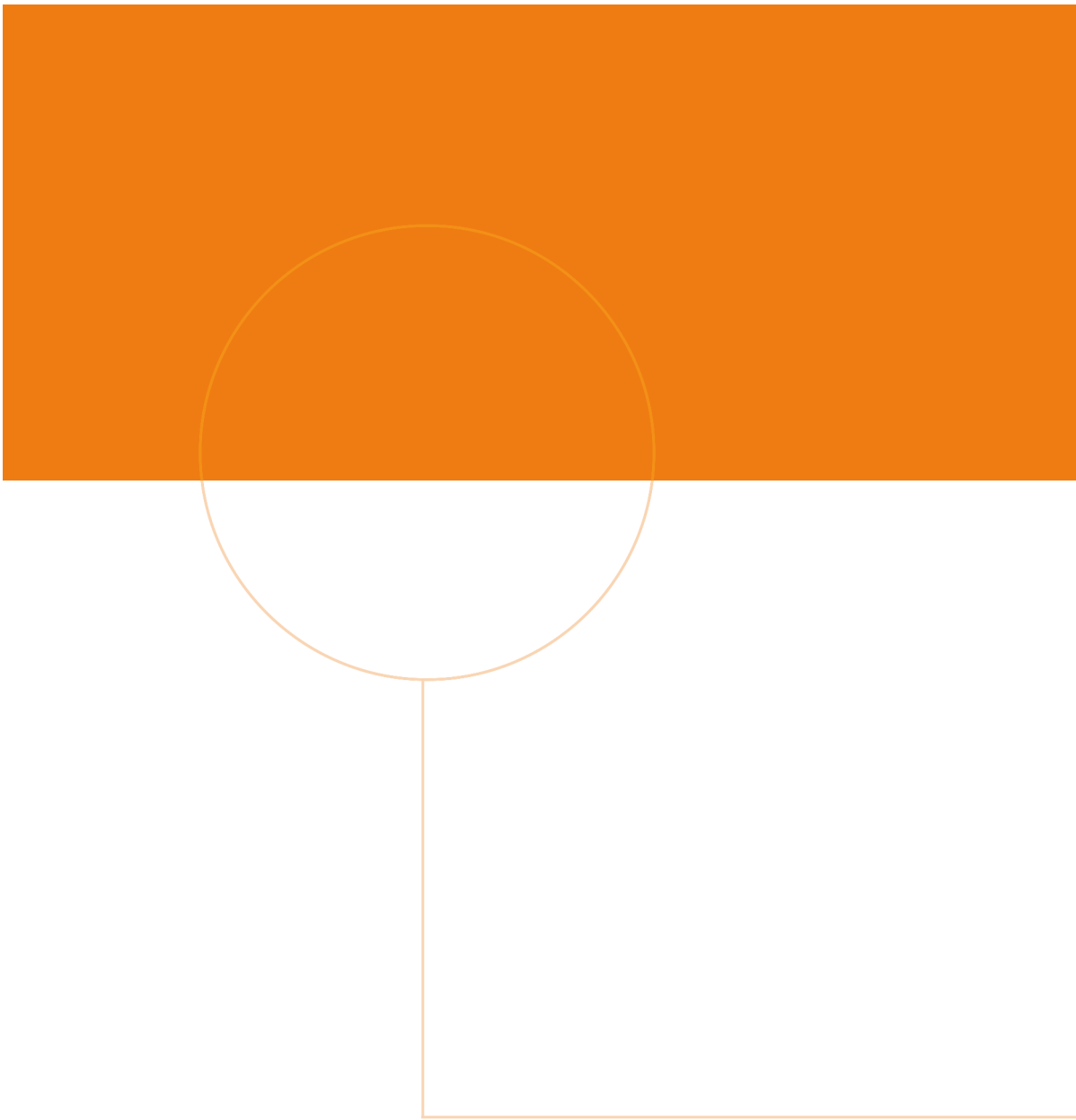

NTNU

Norwegian University of
Science and Technology